

Applications of Niobium Based Materials

FUNDAMENTALS OF NIOBIUM BASED SUPERCONDUCTORS

Yoshio Furuto

The Furukawa Electric Company
Central Research Laboratory
Futaba, Shinagawa
Tokyo 142, Japan

Introduction

Superconductivity, discovered by Onnes (1) in 1911, is the total disappearance of resistance at a finite low temperature (transition temperature T_c). The phenomenon is not rare; 25 out of the elements shown in Fig. 1 (2) and over 1000 alloys and compounds are now known as superconductors (3). The appearance of such a large number is quite surprising and challenging. In a historical overview of the research and development of the superconductors, following the works (4, 5) in 1950's a significant breakthrough occurred in 1961 when Kunzler at Bell Labs (6) found Nb_3Sn remained superconducting in magnetic fields in excess of 9 tesla, while carrying high current densities. This truly opened the door to the so-called type II or "hard" superconductors which resulted in the compact, high field superconducting magnets commonly used today. Such an epoch can be seen in Fig. 2 which is a chronological plot (7) of T_c 's in superconductors discovered.

The element with the highest T_c is niobium (9.2 K) and the highest T_c , known so far, is 23.6 K for Nb_3Ge . Commercial superconductors are available based on the two ductile alloys, Nb-Zr and Nb-Ti, although the former has been almost entirely superseded by the latter. A-15 compounds, Nb_3Sn and V_3Ga are also commercially manufactured as conductors. Niobium is used for applications of RF cavity and power transmission cable. Thus, niobium based superconductors are indispensable for the applications of superconductivity such as electrical machinery, magnetically levitated train, high energy physics and so on. Recently, large-scale applications including fusion reactors, MHD power plants and energy storage systems have had a strong impact on the research and development of new or improved superconductors with high critical fields, high current densities and good cost performances. Candidates to meet such needs will no doubt come from the family of niobium based superconductors.

Regarding the fundamentals of niobium based superconductors, an attempt is made in the following paper to summarize the theories and experimental results as well as to make some comments on the future perspective under seven headings: Transition Temperature and Critical Field, Flux Pinning and

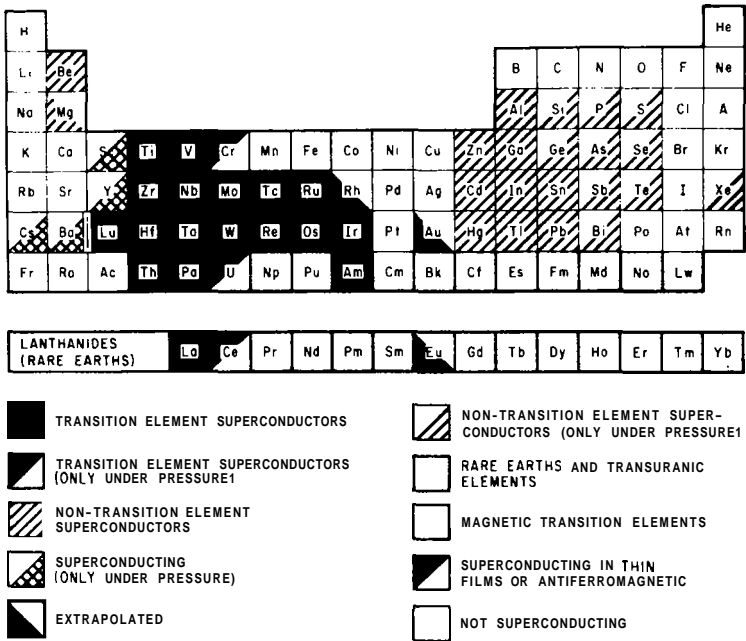


Figure 1. Superconducting elements in the periodic system (3).

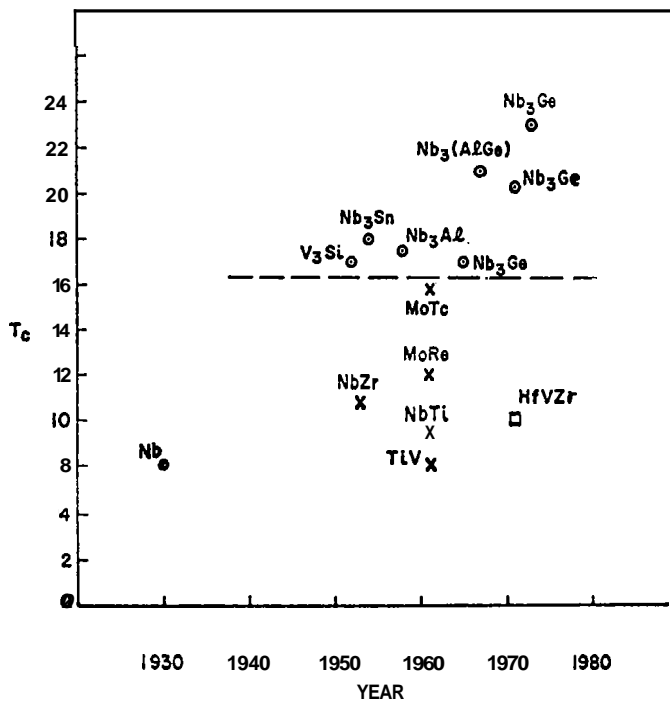


Figure 2. Chronological development of high-T_c superconductors A-15 compounds (open circles) ductile alloy (x) and Laves phase compound (□) (7).

Critical Current, Stabilization, AC losses, Mechanical Properties, Fabrication Methods and Prospects for Superconductors in the Future. Emphasis is made on practical superconductors and recent data.

Transition Temperature and Critical Field

Transition Temperature T

According to BCS theory (8), the energy gap 2Δ and transition temperature T are given by

$$2\Delta = 4\hbar\omega_{ph} \exp \{1/N(0)V\} = 3.52 kT_c \quad (1)$$

where V and N(0) indicate the interaction potential of the superconducting electrons (Cooper pairs) and the density of states at the Fermi level, respectively.

It is possible to make a calculation of T_c of superconductor based on equation (1), if the normal state properties of the material are well understood. Unfortunately, high-T superconductors are least known in the normal state. Predictions of high values of T_c follow from empirical rules formulated by Matthias (9). The rules are

1. Superconductivity occurs only in metallic systems, and never if the system exhibits ferro- or antiferromagnetism.
2. Superconductivity occurs when the electron-to-atom ratio e/a lies between 2 and 8. Nontransition metals show T_c increasing as e/a increases from 2 to 6. Transition metals show a much more complicated behavior, exhibiting peaks at e/a of 4.7 and 6.5, and a sharp minimum in between.

Dependence of T upon the electron-to-atom ratio is related to the effect of the density of states N(0). The value of V would appear to be fairly constant between about 4 and 8 electrons/atom. The effect of crystal structure is not well understood. The A-15 (Cr_3Si type) compounds with the highest T_c 's are those formed between either Nb or V and group IIIA or IV A elements, e/a being 4.5 or 4.75. The high-T B-1 (NaCl type) compounds are carbides and nitrides of transition elements, Mo, Nb, Ta and Ti or mixtures of these, e/a being 4.5 or 5.0. The A-12 (a-Mn type), D-8_b (sigma phases) and C-15 (Laves phases) with high T's all have e/a ratios close to 6.5, the second most favorable value. The classification of high T superconductors is shown in Fig. 3.

Ductile alloys were rather thoroughly investigated over a decade ago and there has been no advance in T's recently. On the other hand, progress is steadily being made in raising T of compound superconductors. This is not due to the discovery of new superconductors, but rather *to* the application of new methods of fabricating already known A-15 compounds. Let us take Nb_3Ge , T_c of which was raised up to 17 K in 1965 by Matthias (10) using rapid

High T_c High H_c Superconductors

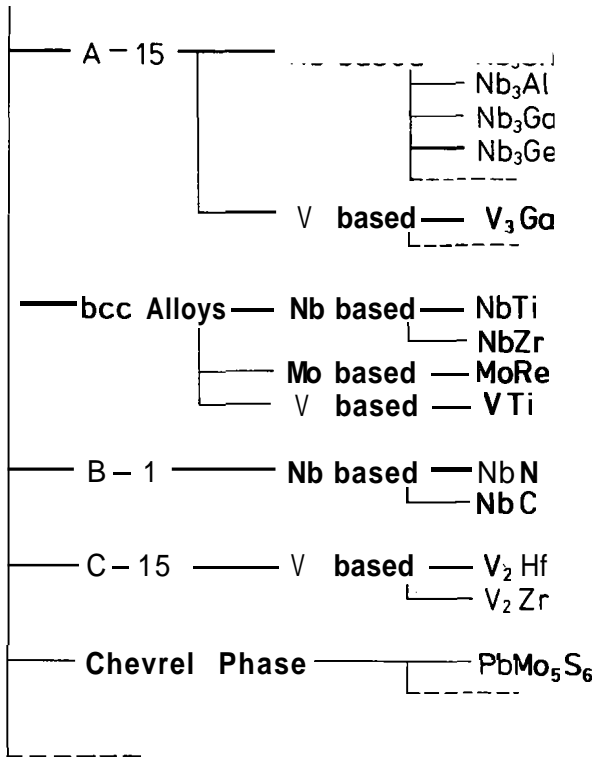


Figure 3. Classification of high-T_c superconductors.

quenching techniques. In 1973 Gavaler (11) obtained 22 K by utilizing a sputtering method. The latest and highest T_c for Nb₃Ge is 23.6 K by Paidassi et al (12). Table I shows the latest T_c's for A-15 compounds (12, 13).

The prediction of a value of T_c for a new member of an already known class can only be carried out by extrapolation of empirical correlations between experimental T and material properties. Dew-Hughes (14) derived the following empirical equation for A-15 compounds based on McMillan's theory (15).

$$T_c = 27.5 (T_A - 2) / \sqrt{M_B} \quad (2)$$

$$T_c = 19.6 T_A C(A) / \sqrt{M} C(A-15) \quad (3)$$

where T_A is T_c of A atom, M_B mass of B atom, M mean atomic mass of compound; C(A) and C(A-15) are atomic volumes of atom A and A-15 compound, respectively. By using the equations, he obtained 38- 25.4 K of T_c for Nb₃Si. **High T** above 30 K may be attained with Nb₃Si in the near future.

Table I. $T_c(K)$ for A-15 compounds formed between Va and VIb elements.

Va \ IVb	Sn	Ge	Si
V (5.3)	4.3	11.2	17.1
Nb (9.2)	18.3	23.6	?
Ta (4.5)	6.4	8.0	8.6

Upper Critical Field H_{c2}

When a superconductor with the Ginzburg-Landau parameter $\kappa > 1/\sqrt{2}$ (type II superconductor) is subjected to an externally applied field, it shows a Meissner (16) effect (exclusion of magnetic flux from the body of a superconductor) up to the lower critical field H_{c1} . At this field normal regions are nucleated at the surface of the superconductor. Those regions carry magnetic flux and move into the body. The superconductor is now said to be in the mixed state. As the external field is raised, more of these normal regions are nucleated. At some high field the normal regions are so densely packed within the superconductor that they begin to overlay and the normal state is achieved. This field is the upper critical field H_{c2} . According to GLAG theory (17), the expressions for H_{c1} , and H_{c2} are given by

$$H_{c1} = (H_c / \sqrt{2} \kappa) (\ell_n \kappa + 0.08) \quad (4)$$

$$H_{c2} = \sqrt{2} \kappa H_c \quad (5)$$

GL parameter κ is related to the normal electron mean free path ℓ and consequently the normal state resistivity ρ_n . Thus, both κ and H_{c2} can be expressed in terms of ℓ and ρ as follows (18):

$$\kappa = \lambda / \xi = \lambda_L / \ell = \kappa_0 + 2.37 \times 10^6 \gamma^{1/2} \rho_n \quad (6)$$

$$H_{c2}(0) = 3.11 \times 10^3 \gamma \rho_n T_c \quad (7)$$

where λ is the penetration depth, ξ the range of coherence and γ the Sommerfeld constant, the temperature coefficient of electronic specific heat. An increase in normal state resistivity will increase κ and H_{c2} .

H_{c2} 's for high field superconductors are listed in Table II (14). The highest H_{c2} ever measured is 60 tesla for $PbMo_{5.1}S_6$ (19). Theoretical estimates of H_{c2} are very close to the experimental values except for the vanadium based A-15 compounds and some of bcc alloys. Experimental H_{c2} 's of the vanadium based A-15 compounds, and V 40 at.% Ti and Nb 70 at.% Ti bcc alloys are lower than those derived theoretically because they suffer a paramagnetic limitation (Clogston limitation (20)). Nb based A-15 compound and $PbMo_{5.1}S_6$ can escape the paramagnetic limitation because of spin-orbit coupling induced electronic spin-flip scattering (21). Spin-flip scattering is most effective in materials of high resistivity with atoms of large atomic mass.

Table II. Upper critical fields for high-field superconductors.

Superconductors	T_c (K)	$H_{c2}(0)$ theor (T)	$H_{c2}(0)$ expt (T)
bcc alloys			
V 49 at. % Ti	7.0	24.0	11
Nb 37 at. % Ti	9.2	10.1	9.6
Nb 56 at. % Ti	9.0	15.7	14.1
Nb 70 at. % Ti	7.2	17.5	14
Nb 25 at. % Ti	10.8	8.6	9.2
B1 (NaCl) compounds			
NbN	15.7	13.5	15.3
Nb(C_{0.3}N_{0.7})	17.4	-	11
A15 (Cr ₃ Si) compounds			
V ₃ Ga	14.8	14.9	25
V ₃ Si	16.9	34.0	24
Nb ₃ Sn	18.0	29.6	28
Nb ₃ Al	18.7	32.7	33
Nb ₃ Ga	20.2	34.1	34
Nb ₃ Ge	23.6	37.1	38
Nb₃(Al_{0.7}Ge_{0.3})	20.7	44.5	43.5
Ternary sulfides			
PbMo_{5.1}S₆	14.4	59.9	60

In this connection, the ternary or quaternary systems with heavier elements are advantageous in getting higher H_{c2} 's compared to the binary systems and are expected to add the effect of shorter electron mean free path on higher H_{c2} 's for some cases. Fig. 4 shows the critical field map for the ternary alloy of Nb, Ti and Ta by Suenaga and Ralls (22). Some enhancement in H_{c2} (4.2 K) is seen in the figure. Table III shows T_c and H_{c2} (4.2 K) of Nb-Hf/Cu-Sn and Nb-Hf/Cu-Sn-Ga by Tachikawa et al (23). H_{c2} 's of composite processed Nb_3Sn are significantly increased by the addition of Hf to the Nb core and Ga to the matrix, despite small increases in T_c .

Flux Pinning and Critical Current

Theories of Flux Pinning

Flux lines in the mixed state of a type II superconductor experience a Lorentz force $F_L = J \times B$ whenever a current flows in the superconductor. The force acts in a direction normal to both the flux lines and the current. If the flux lines are able to move under action of this force, they will dissipate energy and the superconductor will show an induced resistance. It is possible to "pin" the flux lines and prevent them from moving by interaction with the microstructural features of the material, and a pinning force F_P is exerted on the flux lines. The critical current density J_c is such that the Lorentz F_L is just balanced by this maximum pinning force as given below (24, 25).

$$J(B, T) \times B = F_P(B, T) \quad (8)$$

Pinning is due to crystal lattice defects, such as dislocations found in heavily cold-worked materials, impurities and precipitates of a second phase. The critical current is not an intrinsic property of a particular composition, but a so-called structure-sensitive property and is strongly influenced by the sample's metallurgical history.

Many empirical expressions have been proposed to describe the relation between F_P and B . Theoretical and experimental results are often expressed in the general form $F_P(h) \propto H_{c2}^n(T) f(h)$ where h is the reduced field, H/H_{c2} . The pinning forces, for example, for normal particles or the one with the change in κ are given below (26).

$$F_P = \mu_0 \frac{1}{4} H_{c2}^2 \frac{\Delta\kappa}{\kappa^3} \frac{V}{\xi} (1-h) n_V \quad (a < \xi) \quad (9)$$

$$F_P = \mu_0 \frac{1}{4} H_{c2}^2 \frac{\Delta\kappa}{\kappa^3} \pi \xi a (1-h) n_V \quad (a > \xi) \quad (10)$$

where a is diameter of the particle and n_V the total number of pinning interactions per unit volume. If L , the average distance between pinning centers, is $> d$, the inter-flux-line spacing, then all pins are occupied by flux line and $n_V \sim 1/L^3$, the pin density. If $L < d$, $n_V \sim B/L \phi_0$. For large precipitates, F_P is given by (27).

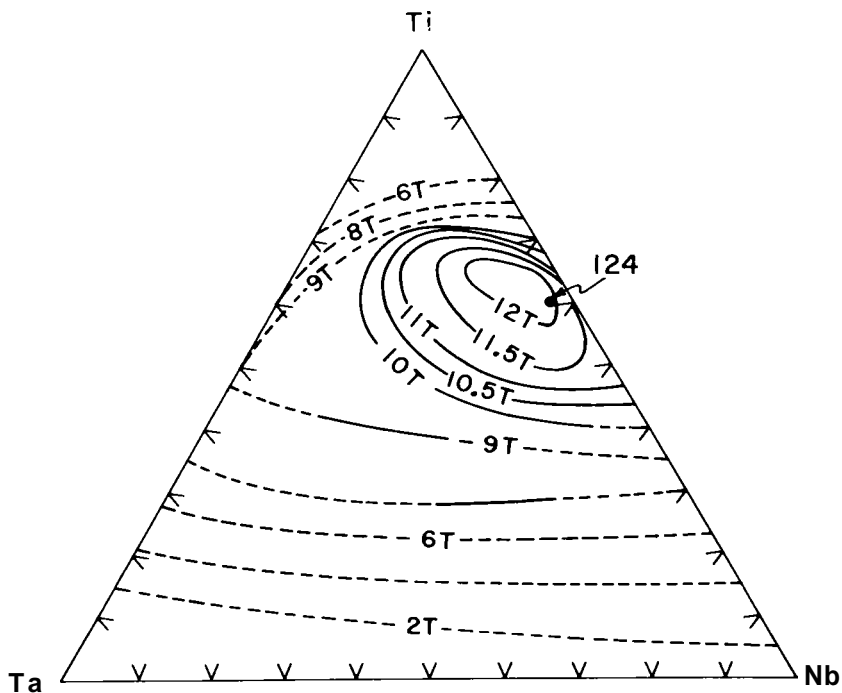


Figure 4. Critical field map for Nb-Ti-Ta alloy (22).

Table III. T_c and $H_{c2}(4.2\text{ K})$ of Nb-Hf/Cu-Sn and Nb-Hf/Cu-Sn-Ga compounds (23).

Specimen	Heat treatment ($^{\circ}\text{C} \times \text{hr}$)	T_c (K)	$H_{c2}(4.2\text{K})$ (T)
Nb/7Sn	800 x 100	17.1	19
2Hf/7Sn	800 x 100	17.5	21
5Hf/7Sn	800 x 100	17.6	23
Nb/5Sn-4Ga	800 x 100	17.4	21
2Hf/5Sn-4Ga	800 x 100	17.7	25
5Hf/5Sn-4Ga	800 x 20	17.7	25
5Hf/5Sn-4Ga	800 x 100	17.7	25.5
Nb/3Sn-9Ga	800 x 100	17.6	23
5Hf/3Sn-9Ga	800 x 20	18.0	26

$$F_p = \frac{\mu_0 S_v H_c^2 h^{3/2} (1-h)_{AK}}{2\kappa} \quad (11)$$

where S_v is the surface area of grain boundary per unit volume α (grain diameter)⁻¹. Kramer (28) has suggested that the ultimate pinning force that can be exerted must correspond to the shear strength of the flux-line lattice. The shear strength, at high fields, is proportional to $h^{1/2}(1-h)^2$, going to zero at H_{c2} ($h=1$) as shown in Fig. 5. Such a trend has been found for many materials (14) (Fig. 6).

Critical Current Density of Nb-Ti Alloys

In the Nb-Ti alloys which form the basis for many commercial materials, $J(H)$ is enhanced by cold work. This is probably due to the refinement of the dislocation cell structure and the presence of a high dislocation density. Fig. 7 shows $J(H)$ at 5 tesla versus inverse cell sizes of Nb-Ti alloys (29). $J(H)$ increases with increased reciprocal of sub-band diameter.

It is also enhanced by a precipitation heat treatment for some field range. Once effective pinning centers in the form of α -phase precipitates have been formed, the pinning force is controlled by the cell size. The highest J values are obtained when the cold area reduction is greater than 90%, thereby indicating that the dislocation networks act as nucleation sites for the α phase. Fig. 8 shows a typical behavior of Nb-45 wt.% Ti (30) in which cold area reduction is initially followed by heat treatment and then further cold area reduction. Another example of remarkably increased I with cold reduction after final heat treatment for Nb50 wt.% Ti is shown in Fig. 9 (31).

It is reported that a heat treatment in two steps may yield more effective pinning centers than the conventional single ageing treatment. (See Fig. 10 (32)). The first step being ageing for long time at the temperature at which a large number of fine precipitates exist stable and the second step being ageing for short time at the elevated temperature for the growth of precipitates. Fig. 11 shows $J(H)$ versus temperature curves for Nb-Ti based alloys containing 8 wt.% and 25 wt.% T_a (33). These alloys are favorable for use at fields around 12 tesla and at temperatures below 2 K.

Critical Current Density of Nb₃Sn Compound

Pinning in A-15 compounds is produced by a fine grain size and by precipitates. It is difficult to distinguish between the two effects since the presence of precipitates will cause refinement of the grain size.

Much of the critical current data generated on bronze-processed Nb₃Sn has been interpreted in terms of flux-pinning interaction with grain boundaries. J_c of Nb₃Sn at high fields is confirmed to be inversely proportional to its grain size down to $\sim 500 \text{ \AA}$ as shown in Fig. 12 (34).

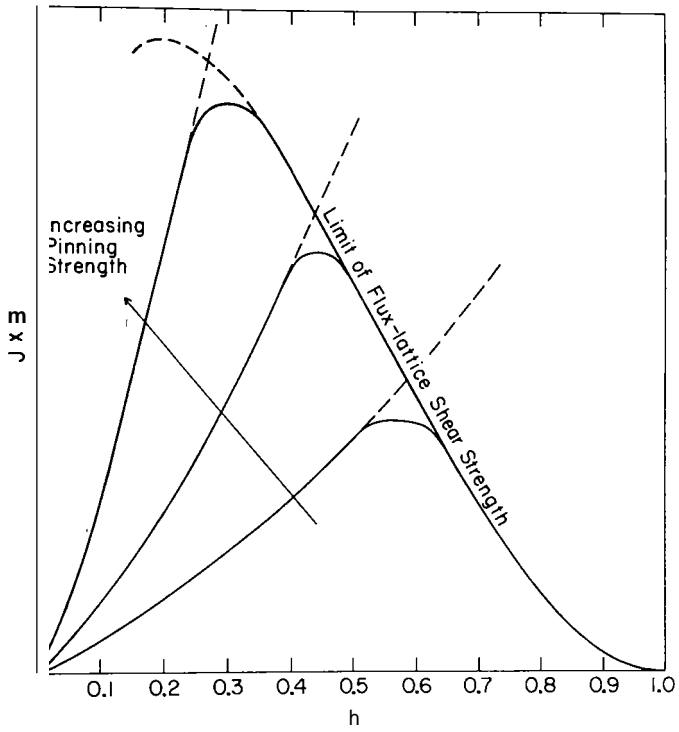


Figure 5. Kramer's flux-shear theory.

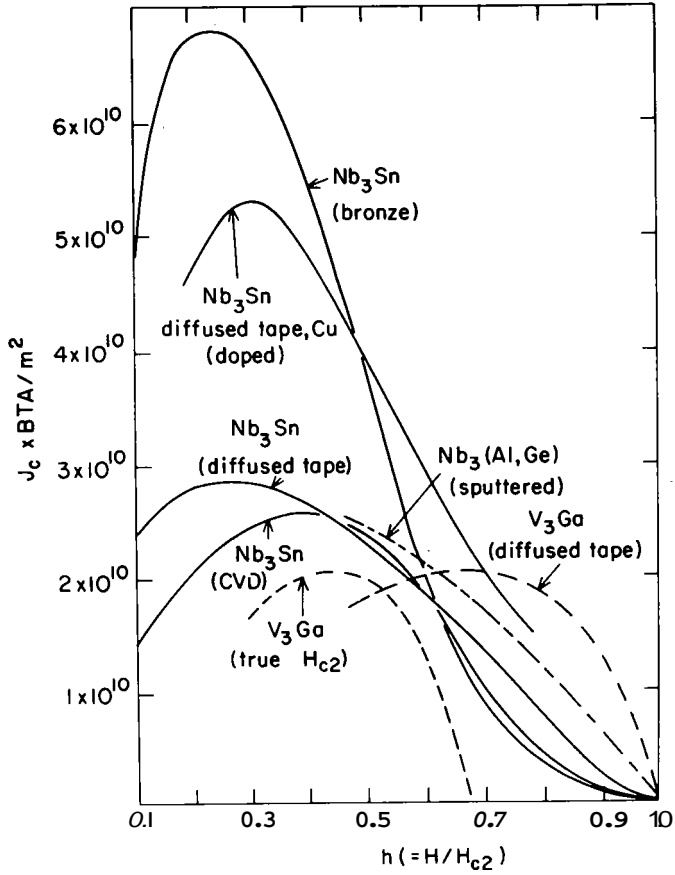


Figure 6. Lorentz force (J_cXB) versus reduced field h for A-15 compounds (14).

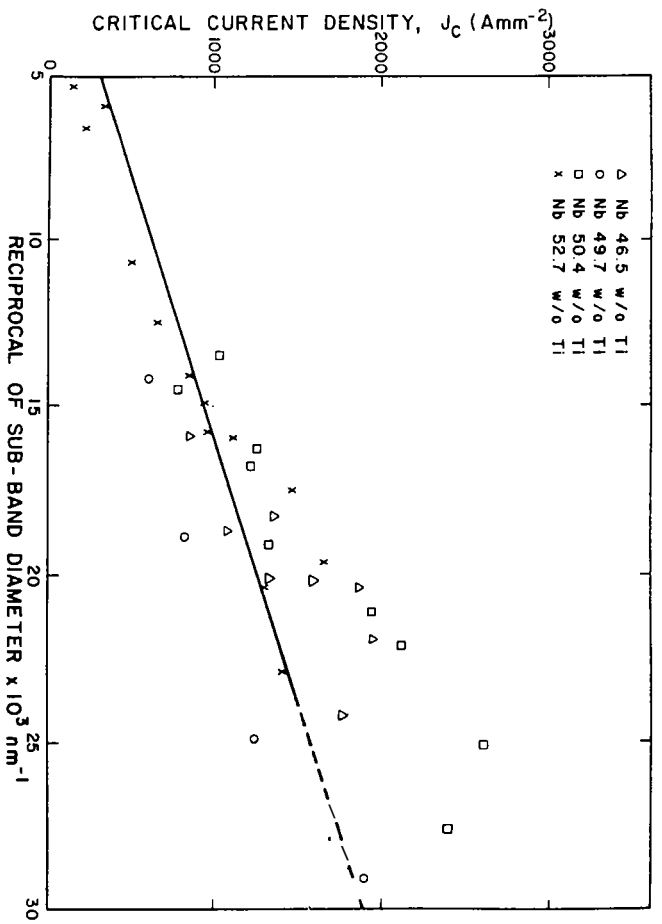


Figure 7. J_c at 5 tesla versus inverse cell size for multifilamentary conductors (29).

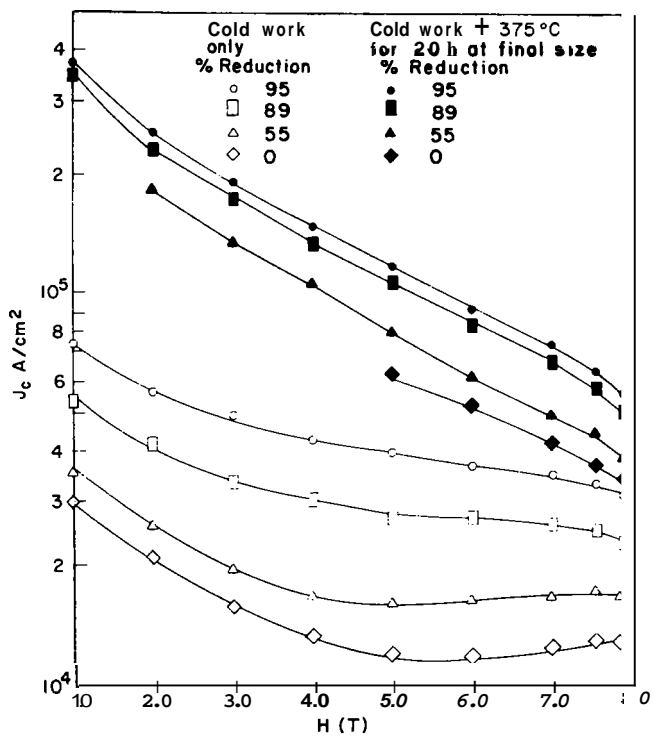


Figure 8. J_c versus applied field for various samples of Nb 45 wt.% Ti (30).

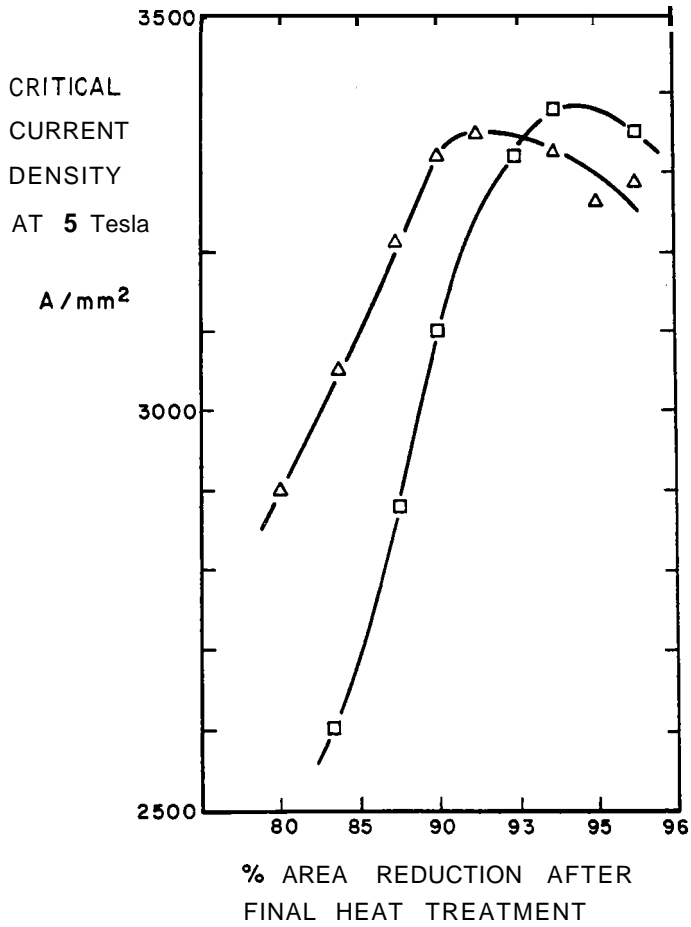


Figure 9. J_c versus cold area reduction after final heat treatment for Nb50 wt.% Ti (31).

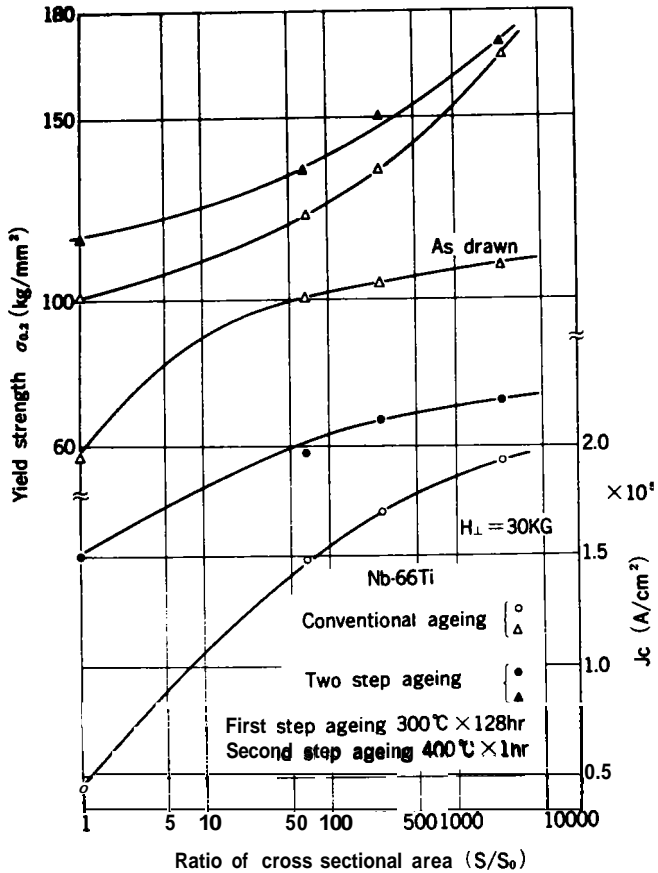


Figure 10. Effect of two-step ageing on Jc and yield strength of Nb66 at.% Ti.

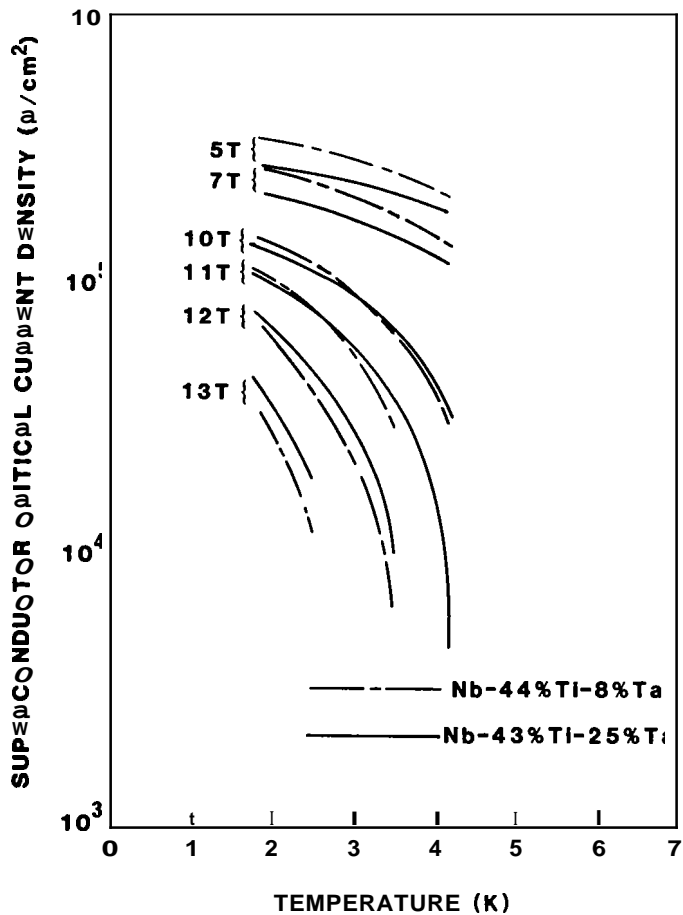


Figure 11. Comparison of two Nb-Ti-Ta alloys (33).

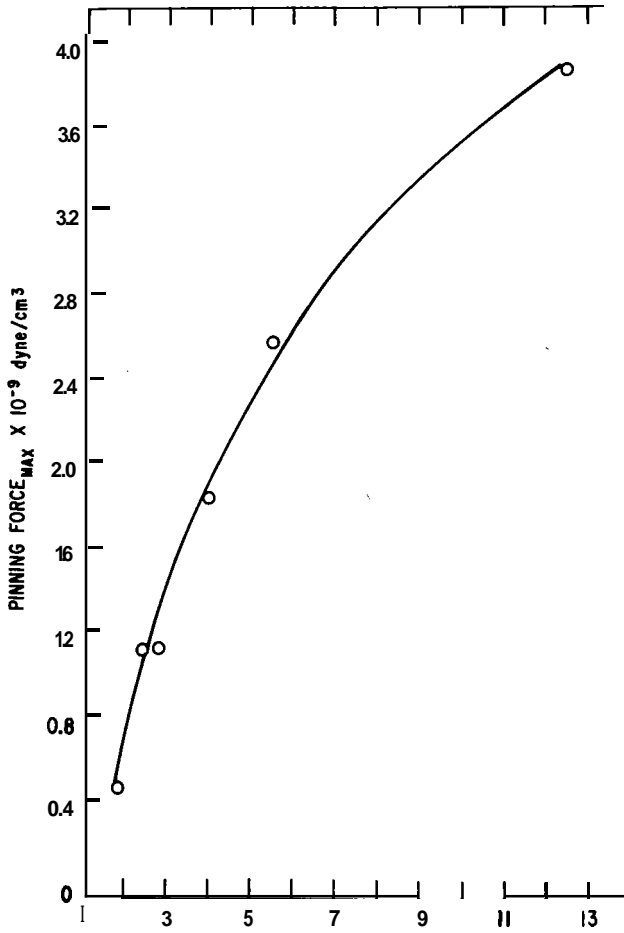


Figure 12. Pinning force maxima versus inverse grain size for multifilament Nb₃Sn wire (34).

Precipitates have been introduced via the substrate or by the presence of oxygen and nitrogen during the reaction to form the compound. Oxides and nitrides precipitate on a substructure within the grains; the highest critical currents are given by oxide particles $\sim 50 \text{ \AA}$ in diameter at a spacing of 200 \AA (35).

Several attempts have been made to increase the high-field performance of Nb_3Sn by raising its critical field H_{c2} , J_c of Nb_3Sn at fields above 12 T is increased by the small addition of Ga ($\sim 2 \text{ wt.}\%$) to the Cu-Sn bronze as shown in Fig. 13 (36). J_c of Nb_3Sn in high fields is also increased by the addition of Hf to Nb core and more significantly increased by the simultaneous addition of Hf to Nb core and Ga to the matrix (see Fig. 14 (23)).

Stabilization

Instability

Magnetic instabilities or flux jumps are a feature of type II superconductors. The motion of flux in a type II superconductor is a dissipative process and causes a local rise in temperature. The pinning force usually decreases as the temperature increases (dJ/dT is negative), more flux is able to move and a small flux change can run away and develop into flux avalanche or flux jump. Such a process is represented in Fig. 15. If this cycle is not halted, the temperature rise will ultimately be large enough to cause the superconductor to exceed its critical temperature and become normal. Note that the stored electromagnetic energies are $10^7 - 10^8 \text{ Jm}^{-3}$ whereas only $10^3 - 10^4 \text{ Jm}^{-3}$ are needed to quench the superconductor.

The normal state can also be directly induced by an external temperature pulse ΔT which may be generated by friction if the superconductor moves under the action of electromagnetic forces. Displacement of only 10μ at 6 tesla produces $1.8 \times 10^4 \text{ Jm}^{-3}$ which will raise the temperature of a typical NbTi/Cu composite from 4.2 to 7 K, probably quenching the magnet. Another origin of heating is the release of elastic energy consequent upon the cracking of brittle component such as epoxy resin in which the superconductor is potted as a result of the difference in thermal contraction. Released energy can be $1.4 \times 10^6 \text{ Jm}^{-3}$, with the result of a temperature rise up to 19 K (37).

Stabilization Techniques

The simplest method to prevent flux jump is cryostatic stabilization, where sufficient normal metal (stabilizer) is bonded to the superconductor to provide an alternate current path during the transition to a resistive state. The stability criterion is expressed as

$$\alpha = I_c^2 P / A p h (T_c - T_b) \quad (12)$$

where α is so-called Stekly's (38) stability parameter, P is the perimetric length for cooling and h is the heat transfer coefficient between liquid He and the conductor; p and A is the resistivity and the cross-sectional area of

the stabilizing metal, respectively. The composite conductor is fully stable if $\alpha < 1$, and partially stable if the operation is made below $I_r = I_c / \sqrt{\alpha}$ in the case of $\alpha > 1$. Full recovery of the superconductor, after the disturbance, requires that generated heat flux be so low that normal nucleate boiling of liquid He is maintained. If the heat flux exceeds a critical value (0.3- 0.5 W/cm²), film boiling commences and gives a sharp rise in temperature. Recently significant improvements in the critical heat flux have been made by means of grooving and chemical treatment of the stabilizer (see Fig. 16 (39)).

Cryostable conductors are essential for a very large magnet, but their high copper-to-superconductor ratio (10 to 100) and consequently low overall current (at most - 30 A/mm²) make them unsuitable for use in more compact high field magnets. The search for stable conductors containing little stabilizer has led to other methods of stabilization as described below.

Adiabatic or enthalpy stabilization (40). The criterion is based on the concept that the energy dissipated during adiabatic flux jump can be absorbed by the material itself by subdividing the superconductor into many filaments of small cross section. The filament diameter d must be

$$d < (1/J) \sqrt{3 C T_o / \mu_o} \quad (13)$$

where C is the specific heat and $T_o = J_c / (dJ_c/dT)$. For Nb-Ti alloys d is $\approx 40 \mu m$, a size easily achieved.

Dynamic stabilization. This is based on the concept of balancing between the rate of flux motion in the superconductor generating heat and the rate of removal of the heat. A dynamic heat balance is achieved by combining a small amount of pure metal slowing down the flux motion. The filament diameter d is limited to

$$d < (1/J_c) \frac{6K_s T_o}{\rho} \cdot \frac{1-\lambda}{\lambda} \quad (14)$$

where K and λ are the thermal conductivity and space factor of the superconductor, respectively.

Intrinsic stabilization. Intrinsic stabilization is an integrated one containing the previous two concepts. Intrinsically stable conductors consist of a twisted composite wire containing many fine superconducting filaments embedded in a normal metal of high conductivity. Twisting the filaments in the multifilamentary conductor is very important because otherwise they will be electrically coupled in the presence of a changing magnetic field. The maximum pitch length of twisting or transposition $l_p = 4 L_c$ is given by (43)

$$L_c^2 < 2 \lambda \rho J_c w d / B \dot{w} \quad (15)$$

where w is the filament spacing and $B \dot{w}$ the rate of change of applied magnetic field.

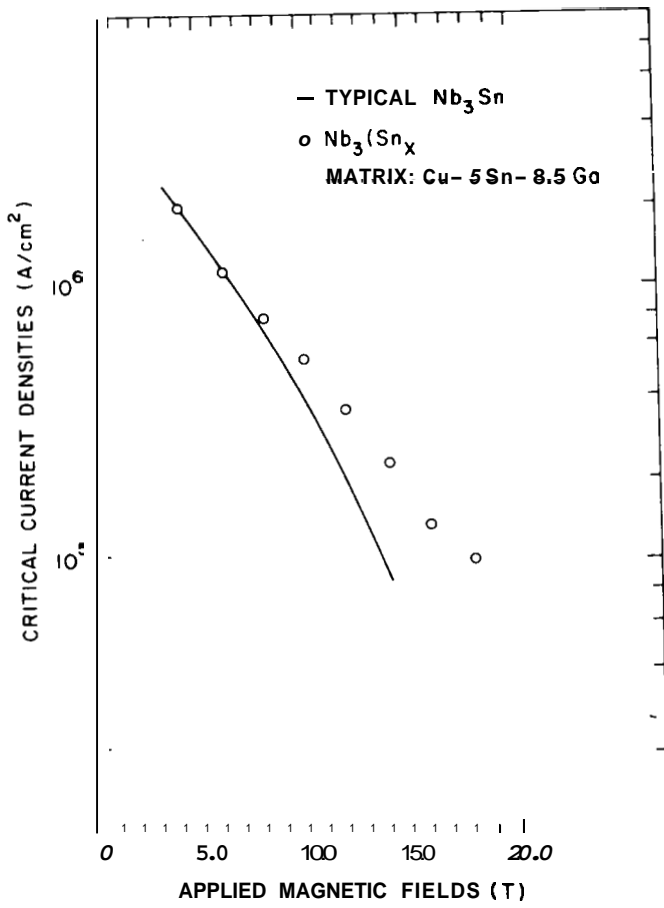


Figure 13. J_c versus applied field for Nb_3Sn and $Nb_3(Sn_xGa_{1-x})$ composite wires (36).

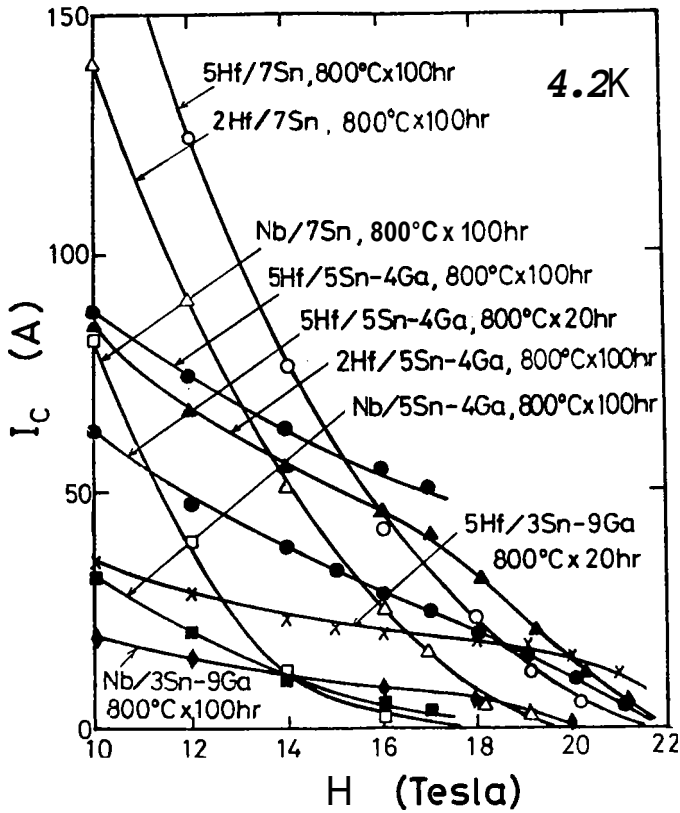


Figure 14. I_c versus applied field for the same samples as in Table III (23).

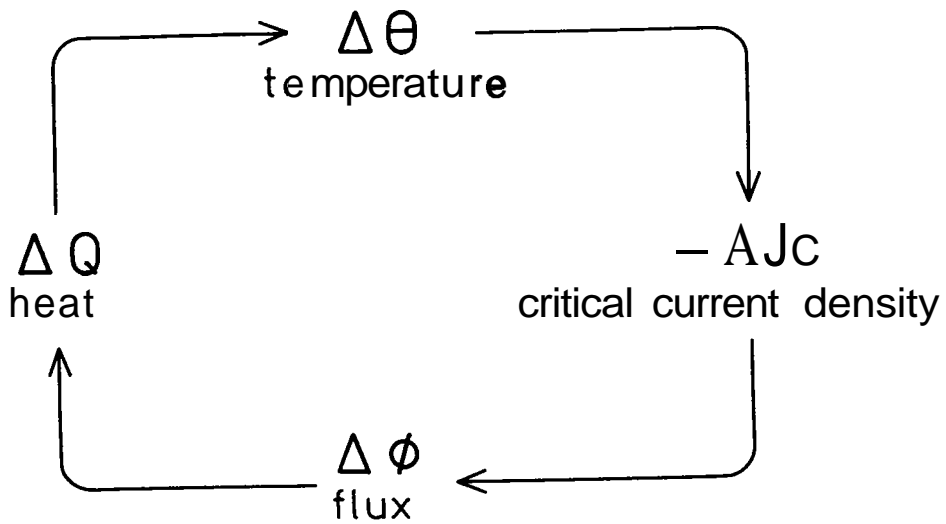


Figure 15. Diagram of instability process.

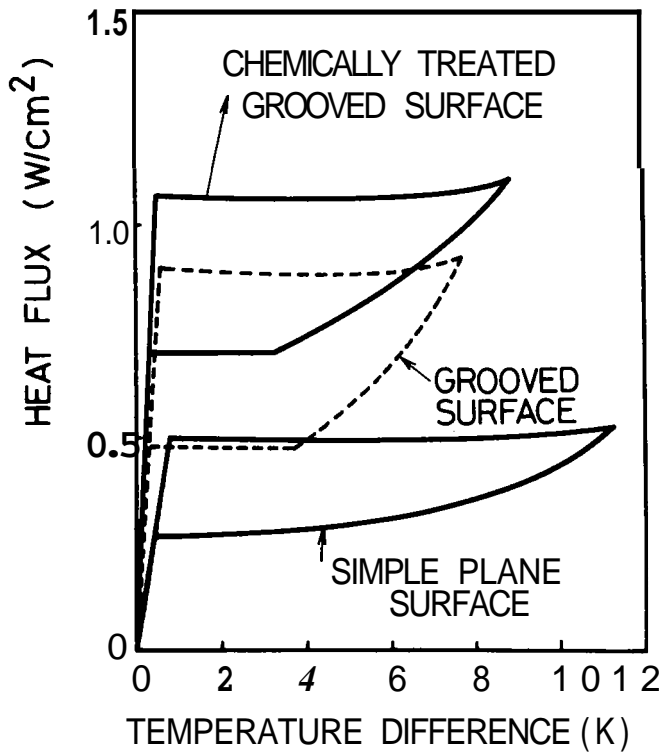


Figure 16. Heat transfer characteristics of various surfaces.

Fig. 17 illustrates practical superconductors in the forms of monolith, cable, braid and hollow conductor depending on the particular magnet applications. Fig. 18 and Table IV are a cross-sectional view of the multifilamentary V_3Ga and Nb_3Sn compound superconductors commercialized for the first time in the world and their specifications (44, 45). With the introduction of filamentary composites, instabilities no longer limit the performance of high-current superconductors. Multifilamentary conductor technology has largely promoted the development of applied superconductivity.

Finally, a few words are appropriate on transient stability. Recent studies suggest that the inclusion of a small portion of liquid helium (-10%) in the magnet windings could provide sufficient transient stability to enable multifilamentary conductor to work well in the presence of mechanical instabilities.

AC Losses

Various Types of AC Losses

Hysteresis loss. Flux pinning leads to magnetic hysteresis. A high critical current superconductor would bring forth loss when subjected to a cyclic external field or carrying alternating current.

For simplicity adopting Bean-London (24) dependence of J_c on magnetic field ($J_c = \text{const}$) among other models (18, 46, 47), hysteretic loss P_c (J/m^3 cycle) is given by

$$P_c = \frac{2\mu_0}{3} \cdot \frac{B_m^3}{J_{cd}} \quad (B_m < B_p) \quad (16)$$

$$= 2\mu_0 J_c B_m \left(1 - \frac{2}{3} \cdot \frac{J_{cd}}{B_m}\right) \quad (B_m > B_p) \quad (17)$$

where B_m is maximum value of alternating magnetic field and $B_p = J_c d$. The hysteretic loss is approximately proportional to the filament size ($2d$) for the field $B_m > B_p$ (~ 0.5 tesla).

Eddy current losses. A changing magnetic field (AC or pulsed) causes the coupling of multifilament conductor when the filaments do not behave as individual filaments and the composite loss exceeds the combined filament loss. This loss is called coupling loss (42) between filaments P_c (Wm^{-3}), expressed as

$$P_c = \frac{\rho_c D^2 B^2}{16\pi} \left(1 - \frac{8}{3\pi} \cdot \frac{d}{D} \cdot \frac{B}{B_c}\right) \quad (18)$$

where d is the filament diameter, D the wire diameter, and $\bar{\rho}_c$ the effective resistivity. In order to reduce the coupling loss, high resistive metal, such as Cu-Ni alloy, is utilized as the barrier between the filaments in addition to heavy twisting of the filaments. For cable or braid, an additional loss between strands is encountered. This is called interstrand coupling loss. The loss is similarly calculated by the equation (18) where d means the strand diameter and D the cable diameter.

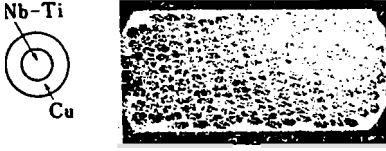
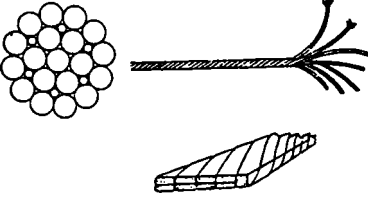


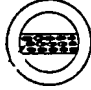
TYPE	CONFIGURATION
MONOLITHIC	
CABLE	
BRAID	
CABLE & BRAID	
HOLLOW	

Figure 17. Various types of conductors.

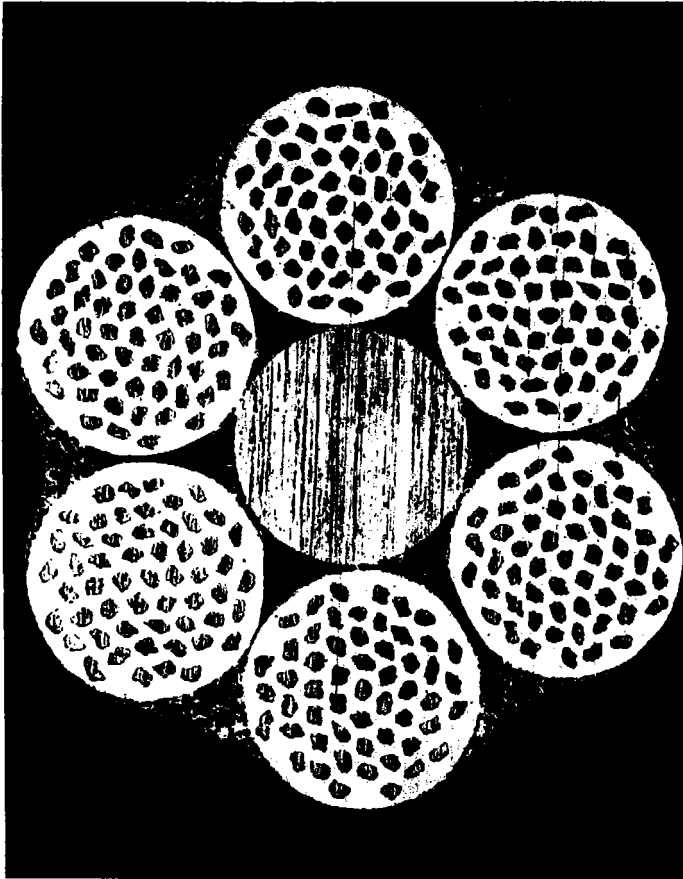


Figure 18. Cross section of multifilamentary compound superconducting wire.

Table IV. Dimensions of stranded multifilamentary compound superconductors.

Superconducting material	Conductor diameter (mm)	Filament diameter	Filament number	Twisting pitch of each strand (mm)	Stranding pitch (mm)
		Filament diameter	Filament number		
V ₃ Ga	0.36	0.010	56 x 6	20	6.5
		0.010	56 x 6		
	0.44	0.010	55 x 8	20	6.5
		0.010	55 x 8		
Nb ₃ Sn	0.36	0.010	55 x 6	20	6.5
	0.44	0.010	55 x 8	20	6.5

The large capacity conductor is usually an assembled one in which superconducting cable or monolith is incorporated into stabilizing housing. In this case, eddy current loss in the stabilizer P (ω_m^{-3}) is given by (48)

$$P_e = (1/2a) \sqrt{2 \omega \mu \rho} B_m^2 (\sinh 2a/\delta - \sin 2a/\delta) / \Delta$$

$$\Delta = \cosh 2a/\delta + \cos 2a/\delta$$

where 2a is width of the stabilizer, ω angular velocity, and $\delta = \sqrt{2 \omega \mu \rho}$ skin depth. Besides those, other AC losses such as self-field loss and loss due to parallel field have been formulated (49, 51).

Experimental Data

Data for power cable (around H₁). Composite Nb/Cu conductors of tubular and flexible structure for power transmission have been developed (52, 54). Fig. 19b presents losses at 4.2 K for Nb clad copper strips measured at Central Electricity Research Laboratories (53).

The loss behavior of Nb₃Sn depends on the method of fabrication and surface treatment. Fig. 20 shows the effects of polishing on the liquid-diffused Nb₃Sn tapes (55). Excellent results can be obtained by electro-polishing.

Data for magnet applications (> A₁). Fig. 21 and Fig. 22 represent typical data of AC losses in various Nb-Ti alloy conductors for pulsed magnets. The specifications of the conductors are shown in Table V (56).

As seen from Fig. 21, hysteresis losses are almost proportional to the filament diameters coinciding with the equation (17). Fig. 22 indicates the advantage of three-component Nb-Ti/Cu/Cu-Ni conductors (TC-B and TC-C) over usual Nb-Ti/Cu conductors at the high change rates of applied field. Fig. 23 shows the effect of conductor direction on hysteresis loss measured by Yamada et al (57) at Fermi Laboratory aiming at superconducting synchrotron (Energy Doubler & Saver Project).

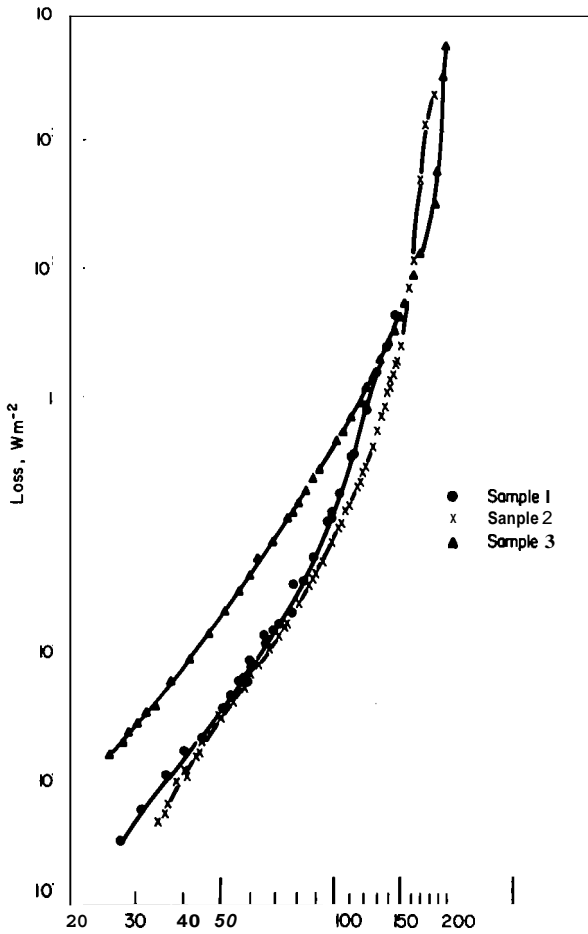


Figure 19. AC loss of Cu/Nb strips (53)
 Sample 1: 17.6 mm wide by 1mm thick, Nb thickness 20 μm
 Sample 2: Identical to sample 1, made from different extrusion
 Sample 3: 8mm wide by 1mm thick, Nb thickness 8 μm

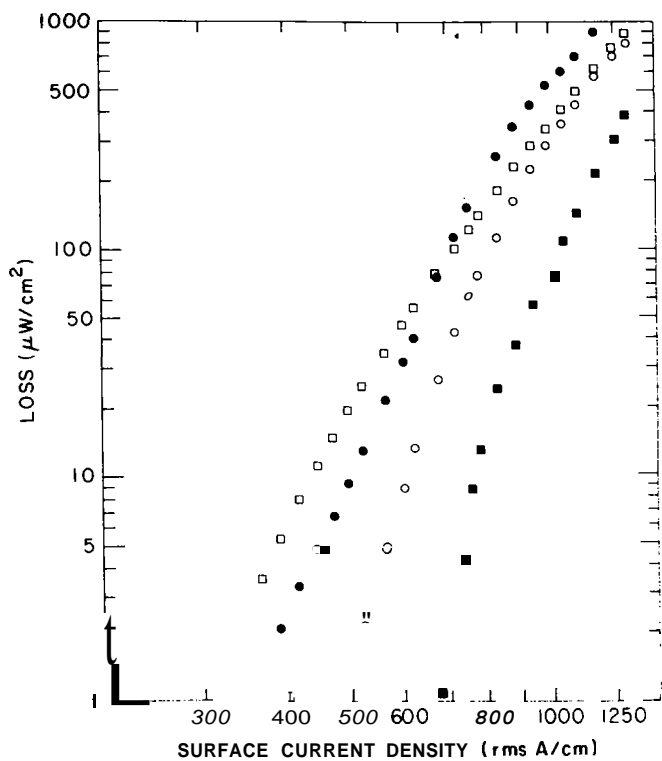


Figure 20. Reduction of loss of liquid-diffused Nb_3Sn tape by polishing. ● as reacted; ○ electro polished; □ mechanical polish; ■ annealed (55).

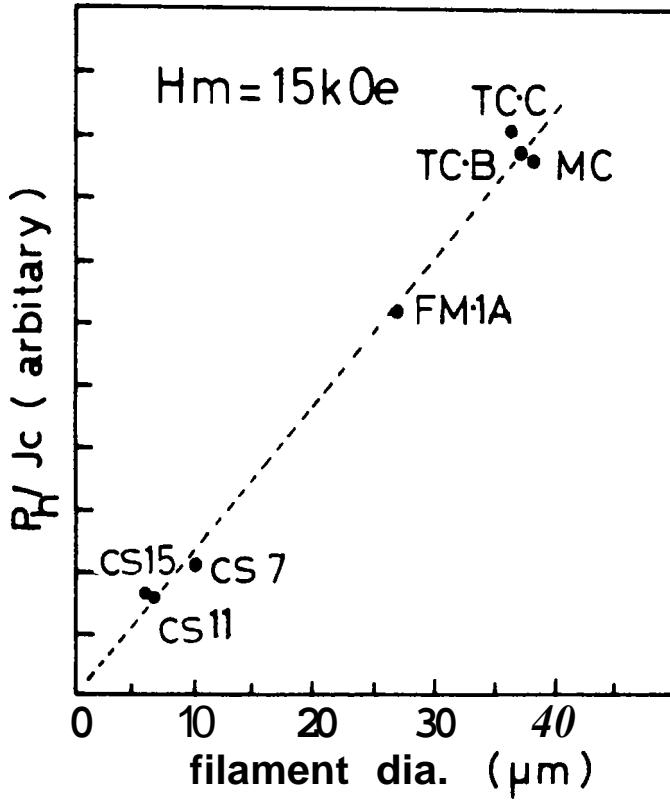


Figure 21. Hysteresis loss versus filament diameter for various Nb-Ti conductors.

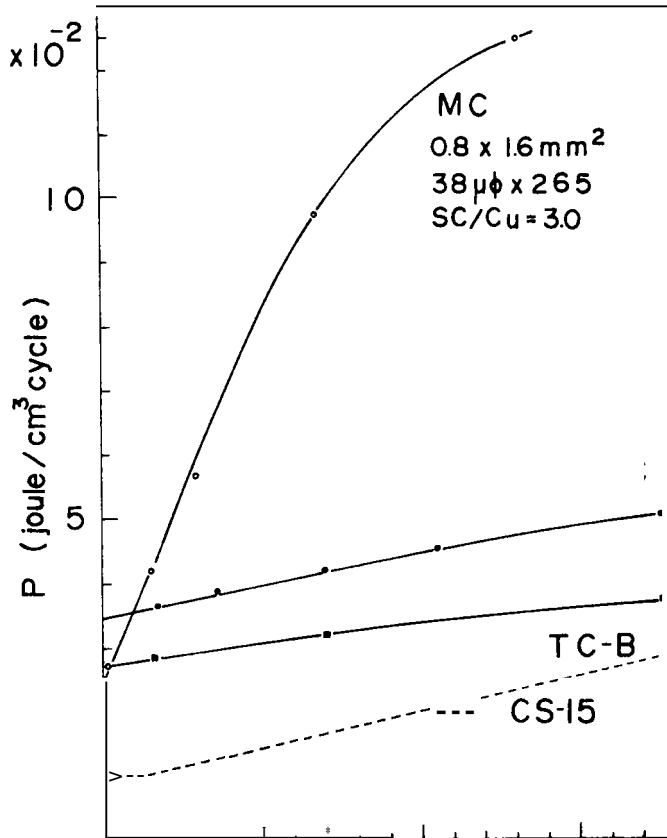


Figure 22. Total loss versus change rate of applied fields for various Nb-Ti conductors.

Table V. Specifications for superconductors for pulsed magnet.

Item	TC-B	TC-C	cs-7	cs-11	CS-15
Conductor size (mm ²)	1.89 x 3.78	1.86 x 3.72	1.91 x 3.81	1.27 x 3.81	0.92 x 4.93
Dia. of strand (mm)	-	-	1.05	0.69	0.59
Number of strand	-	-	7	11	15
Dia. of filament (μm)	37	36	10.3	6.8	6.0
Number of filament	2,300	2,300	21,000	33,000	45,000
Cu to SC ratio	1.8/1	1.9/1	2/1	2/1	1.7/1
Twisting pitch (mm)	25	25	12.5	12.5	12.5
I _C (A) at 5T	3,850	3,840	3,080	2,010	1,900

TC means three-component conductor, and CS compacted stranded cable.

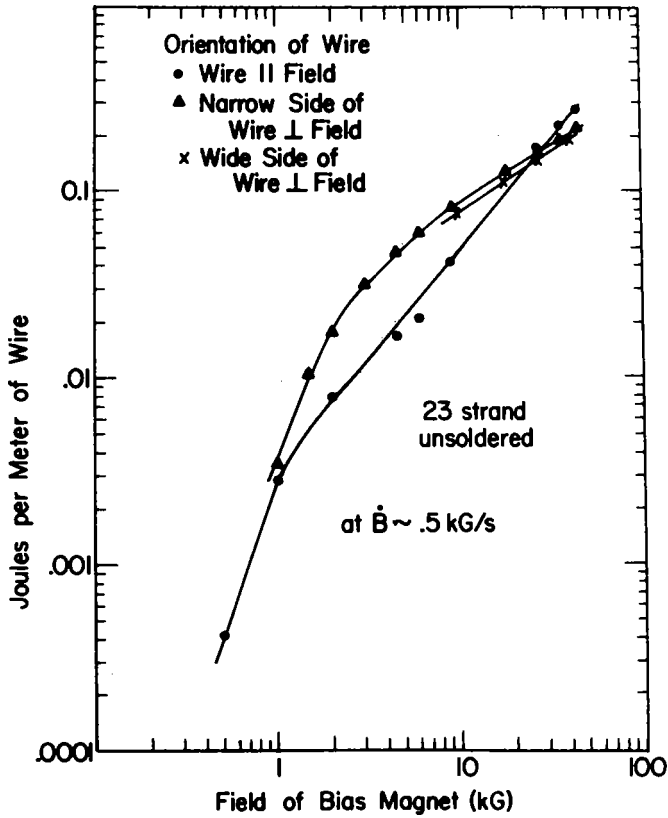


Figure 23. Hysteresis loss versus maximum field at constant \dot{B} (57).

Fig. 24 shows **AC loss** versus frequency of applied field characteristics with twisted and non-twisted cables of multifilamentary Nb_3Sn shown in Fig. 18, indicating the remarkable effect of twisting (45). Fig. 25 also represents the results of **AC loss** measurement by Shen et al (58) of in-situ processed Nb_3Sn wires, indicating the moderate effect of twisting on the hysteresis loss.

Mechanical Properties

Alloy

An extensive compilation by Koch and Easton (59) of Young's Modulus values is shown in Fig. 26. Young's Modulus is seen to decrease as the Ti content of Nb-Ti alloy increases and becomes marked in the range beyond about 50 wt.% Ti, exhibiting a notable increase in electrical resistivity.

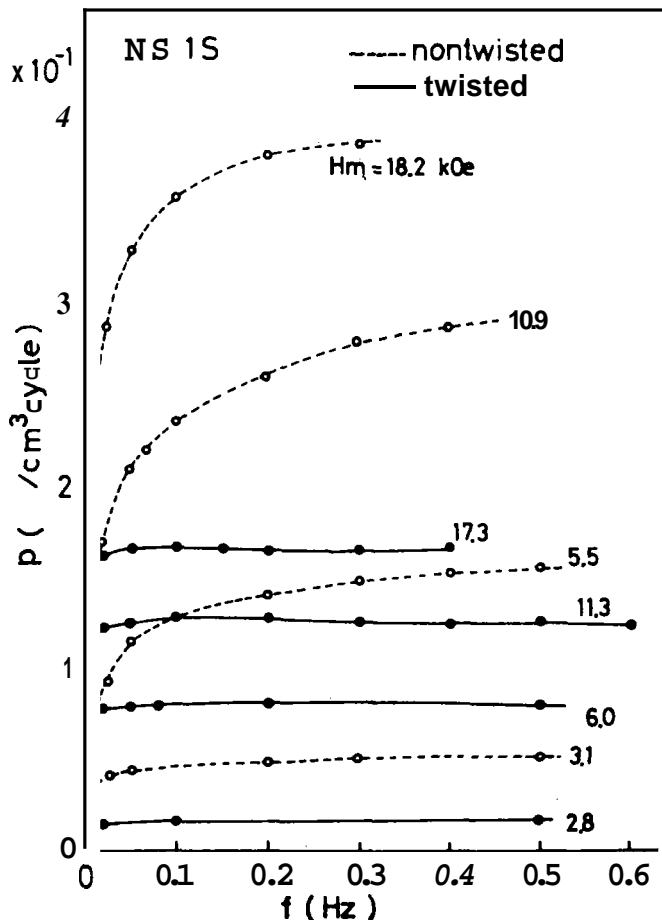


Figure 24. Effect of twisting on AC loss for multifilamentary Nb_3Sn wire.

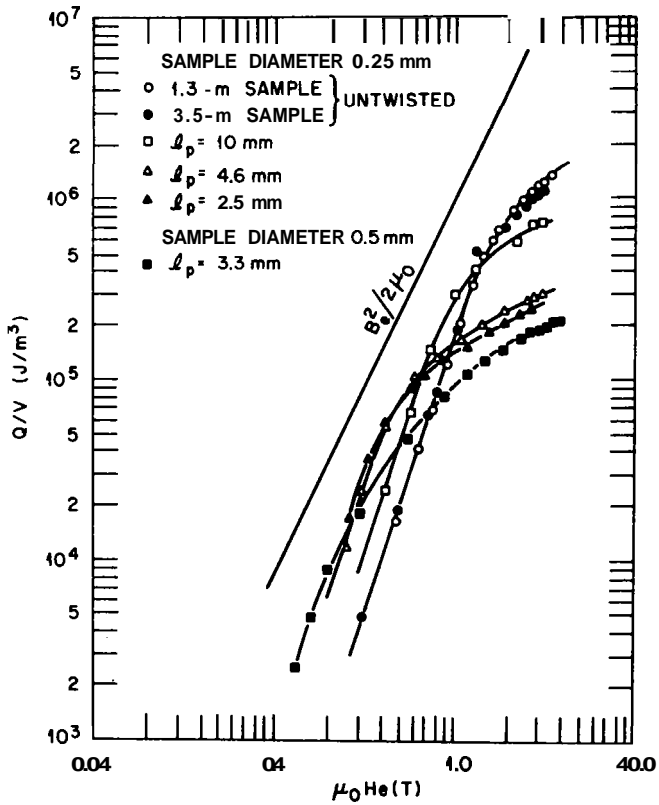


Figure 25. Hysteresis loss for in-situ processed Nb_3Sn composite wires (58).

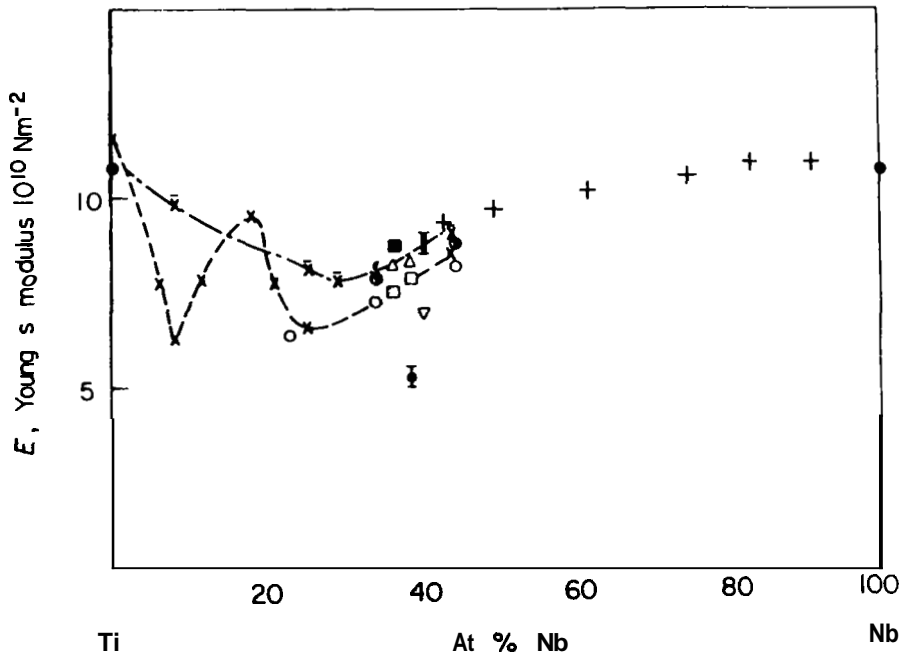


Figure 26. Young's modulus of Nb-Ti alloys (59).

Deformation of a composite such as high-modulus filaments dispersed in a ductile matrix is generally characterized by four stages on a stress-strain plot:

1. Both filaments and matrix deform elastically and the overall modulus is the weighted mean of the individual moduli.
2. The matrix yields while the filaments remain elastic and the overall modulus is now the weighted mean of the filament elastic modulus and the plastic work-hardening modulus of the matrix.
3. Both filament and matrix deform plastically.
4. The composite fails, failure being initiated by filament fracture.

Fig. 27 represents the typical stress-strain curves of the components of a composite (59). A serrated yielding of Nb-Ti filaments is observed in the figure. Table VI shows the specification, and tensile strengths and the elongation measured of a large-capacity conductor with I of over 20 kA at 8 tesla and dimension of 27 mm by 12.8 mm for large D-shaped coil, Figure 28 (60).

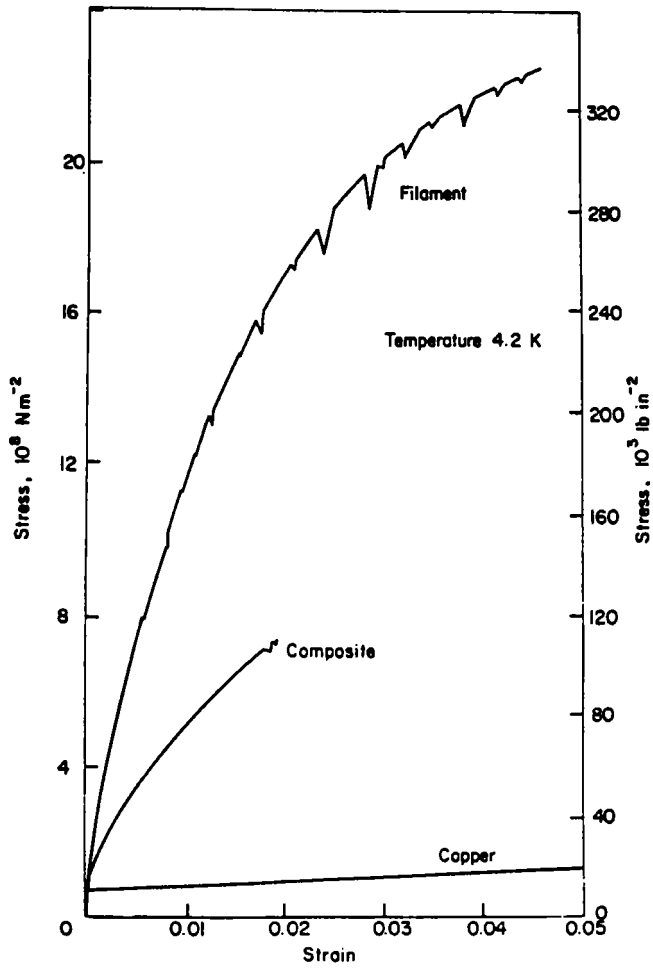


Figure 27. Stress-strain curves for matrix filament, and composite (Cu/Nb-Ti=2.8/1) (59).

Table VI. Parameters of 10 KA conductor for large D-shaped coil.

Item	Specifications	Measured values
<u>Basic parameters</u>		
Conductor size (mm ²)	27 x 12.8	27 x 12.8
Operation current (A)	10,220	10,220
Critical current at 8T (A)	≥ 18,000	20,400
Yield strength at R.T. (kg/mm ²)	≥ 22	25.7
Elongation at R.T. (%)	2-5	6.8
Minimum bending radius (mm)	≤ 200	≤ 200
Equal area heat flux (W/cm ²)	≥ 6.0	~ 0.9
Unit length (m)	200	200
<u>Superconductor</u>		
Cable size (mm ²)	17.1 x 4.3	17.1 x 4.3
Strand diameter (mm)	2.3	2.3
Number of strands	15	15
Cu/SC ratio	1/1	1/1
Filament diameter (μm)	50	50
Number of filaments	1,060 x 15	1,060 x 15
Twisting pitch (mm)	30	30
Stranding pitch (mm)	200	200
Jc of Nb-Ti at 8T (A/cm ²)	>6 x 10 ⁴	7 x 10 ⁴
<u>Stabilizing copper</u>		
Access groove size (mm ²)	17.2 x 4.5	17.2 x 4.5
Cold reduction (%)	2-15	~ 20
Yield strength at R.T. (kg/mm ²)	≥ 34	25.7
Elongation at R.T. (%)	≥ 5	16.3
Resistivity at 8T (Ωcm)	≤6 x 10 ⁻⁸	5.6 x 10 ⁻⁸
Surface work and treatment	Rough surface work	Small grooves plus chemical treatment
<u>Solder</u>		
Soldering material	Pb-Sn	Pb-40Sn

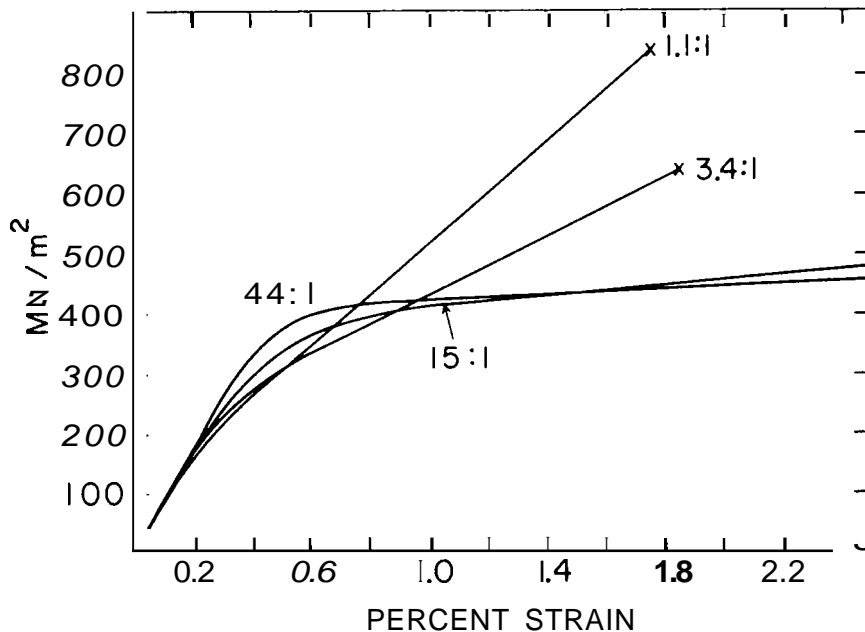


Figure 28. Stress-strain curves for monofilament Nb_3Sn with different bronze-to-niobium ratios (61).

Compound

Due to the brittleness of the compounds, their mechanical strengths and the degradation under strain of their superconducting properties are of great problem on the way to practical applications. A lot of studies on those problems have been performed and phenomenological clarification has been made to a good extent.

Fig. 28 presents typical stress-strain curves for single-filament Nb_3Sn conductors. The first stage out of four is represented by a common elastic modulus of 1.1 GN/m^2 and extends to 0.2% in each case.

The compound in bronze-processed conductors is subjected to a compressive strain originating from thermal contraction of the outer bronze matrix. These compressive strains lower the T_c and J_c of the compounds. In Fig 29, the superconducting transition temperature for a series of single-filament wires is presented as a function of the applied tensile strain (61). The maxima ϵ_m represent the strains at which internal prestrains are removed by tensile loading.

Fig. 30 shows the results of I_c measurements under strain on a Nb_3Sn conductor (62). By choosing the intrinsic strain $\epsilon_0 = \epsilon - \epsilon_m$ as abscissa, extrapolated critical field B_{c2} and normalized critical current I_c/I_{cm} are plotted as shown in (c) and (d), which agrees well with the formula given by (63)

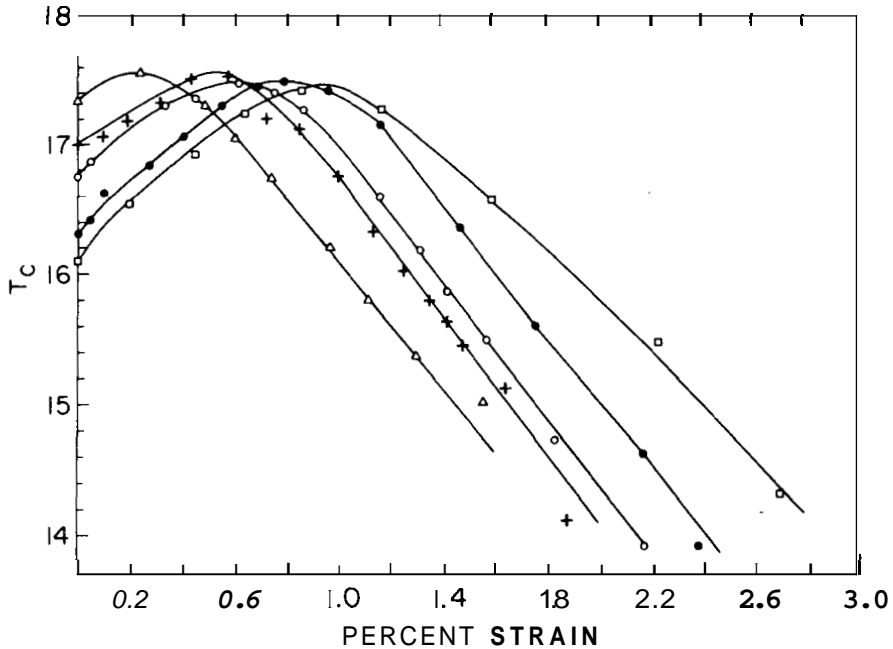


Figure 29. T_c versus strain at 4.2K (61).

$$\frac{I_c}{I_{cm}} = \left[\frac{B_{c2}^*(\epsilon_o)}{B_{c2}^*(0)} \right]^{n-p} \cdot \left[\frac{1-B/B_{c2}^*(\epsilon_o)}{1-B/B_{c2}^*(0)} \right]^q \quad (19)$$

where, for Nb_3Sn , $n \sim 1$, $p \sim 0.5$ and $q \sim 2$.

Fig. 31 shows the results of I measurements under strain and bending of 7.5 KA - 12T Nb_3Sn compacted monolith for High Field Test Facility (HFTF) (64). Fig. 32 also indicates the effects of bending on I of large-current Nb_3Sn conductor with I of 7.7 KA at 10T and cross-section of 17 mm by 10.8 mm for fusion research as shown in Fig. 33 (65). It is noted that I_c/I_{co} monotonically decreases with the bending strain due to the twist pitch being too short for the current to transfer between the filaments.

Fabrication Methods

Here a brief introduction of fabrication methods for superconductors is made, supposing that the next speaker will deal with the theme in detail.

A typical production process for the assembled Nb-Ti conductor, illustrated in Fig. 34, is detailed below.

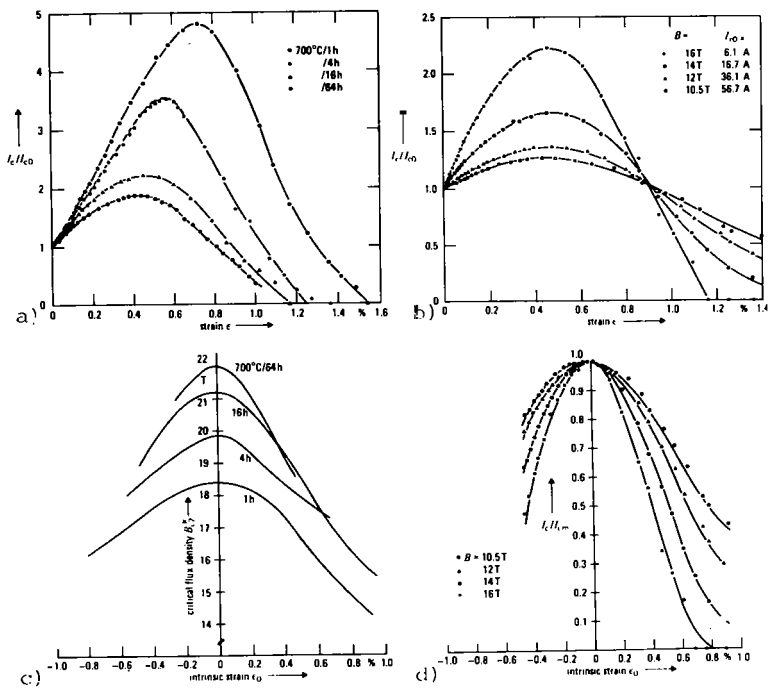


Figure 30. Results of I_c measurement under strains for Nb_3Sn conductor (62).

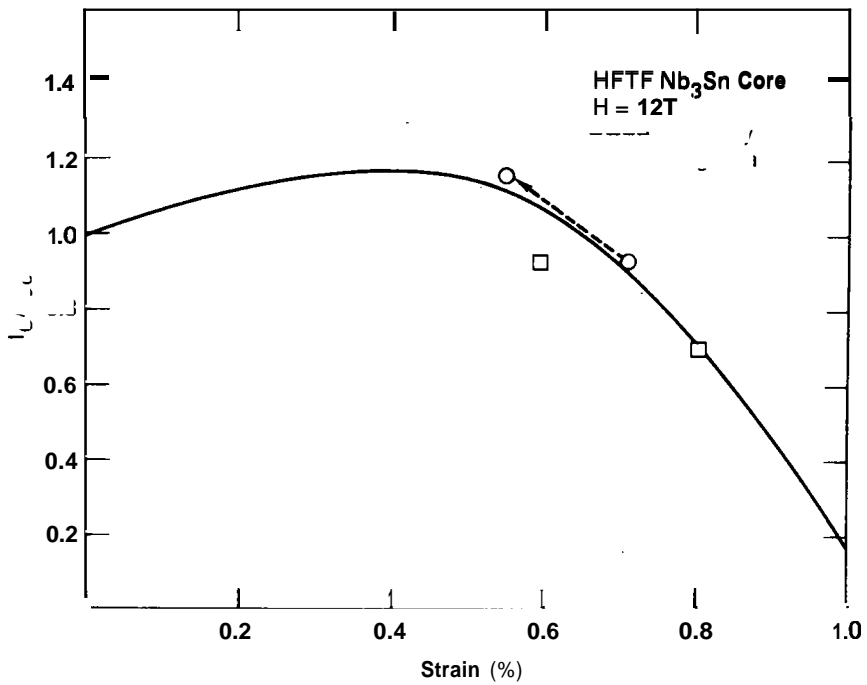


Figure 31. Normalized I_c versus strain for HFTF Nb₃Sn conductor (64).

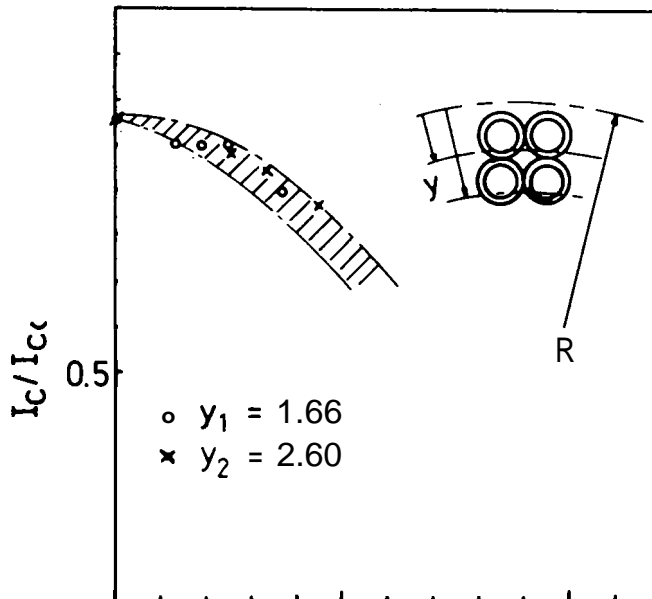


Figure 32. Normalized I_c versus strain for large-current Nb_3Sn cable.

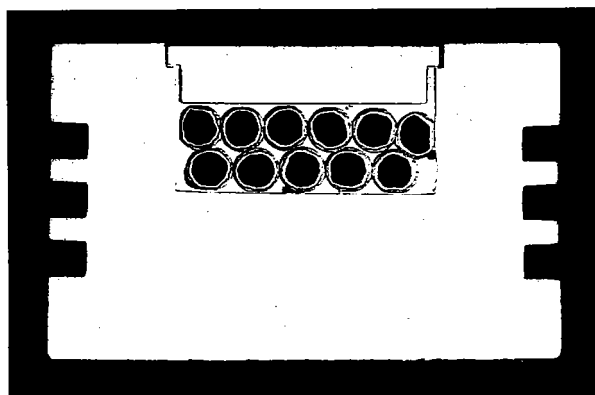


Figure 33. Cross-sectional view of large-current Nb_3Sn conductor.

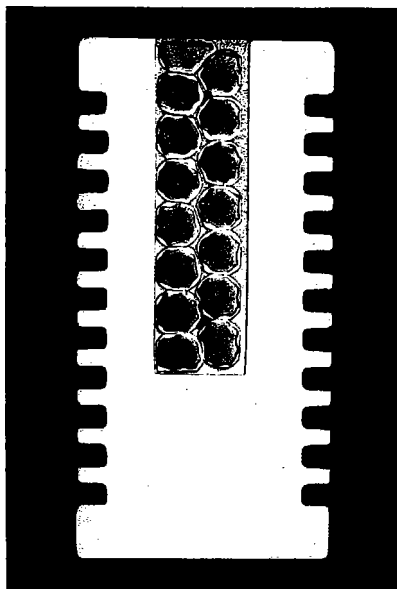


Figure 34. Cross-sectional view of 10 kA conductor for large D-shaped coil.

Superconducting Cable

- S-1. Arc-melting Nb & Ti into Nb-Ti ingot (100- 1,000 kg by weight)
- S-2. Manufacture of Cu clad Nb-Ti composite rod
- S-3. Extrusion of multi Cu/Nb-Ti billet into multifilament rod (200 ~ 300 kg by weight)
- S-4. Rolling & Drawing & Twisting
- s-5. Heat treatment & Pb-Sn solder tinning
- S-6. Cabling & Compaction

Copper Housing

- C-1. Extrusion of OFHC billet into strip (300- 500 kg by weight)
- c-2. Splicing & Drawing
- c-3. Chemical treatment (FC-2)

Assembled Conductor

- A-1. Assembling & Soldering
- A-2. Inspection & Measurement
- A-3. Delivery (3 m-core diameter drum)

The composition of Nb-Ti alloy used is mostly 50 wt.% Ti and, for high field use, 46.5 wt% Ti. Nb-Ti filaments are embedded in OFHC (oxygen-free high conductivity) Cu or mixed matrix of Cu and Cu-Ni by extrusion. The composite is worked into a desirably shaped conductor and heat-treated for precipitation. Various inspections and measurements including those of superconducting properties and bond quality (66) between the filaments are performed.

Secondly, a typical manufacturing process utilizing bronze process for multifilamentary Nb₃Sn superconductors is given in the following.

1. Casting and homogenizing of 10 ~ 14 wt.% Sn bronze
2. Assembly of bronze/61-270,000 cores into billets
3. Hot-working of billets into rods
4. Rod drawing and twisting
5. Wire forming into tape-shaped or compacted stranded conductor
6. Reaction at 600 ~ 750°C for 10 ~ 100 hr
7. Insulation
- a. Testing

The bronze is melted in an inert atmosphere using an electric furnace and cast in iron molds. The composite of the bronze and Nb filaments is made by extrusion. The rapid work-hardening of bronze requires intermediate annealing for every 40- 70% reduction in area. The heat treatment for formation of compound and cooling of the finished composite must be accurately controlled for good superconducting properties to be guaranteed.

Other fabrication methods are listed in Table VII. In-situ process by melting and rapid cooling and powder metallurgy are low cost alternatives to conventional bronze process and applicable to Nb₃Al as well as Nb₃Sn.

Chemical vapor deposition (CVD); and physical vapor deposition (PVD) by sputtering and evaporation have been developed for Nb₃Al, Nb₃(Al, Ge), Nb₃Ge, Nb₃Ga and so on, for which the bronze process does not work well or can not be applicable.

Prospects for Superconductors in the Future

In closing, a few words are paid below in regard to the present state of art and the prospects for superconductors in future.

As far as alloy superconductors are concerned, it may be said, they are coming into the stage of industrial production. The conductors for pulsed magnets for superconductive synchrotron have been already developed and are delivered on a fairly large scale as shown in Fig. 35. The conductors for toroidal field coils and poloidal field coils of Tokamak reactor are under way of research and development. Qualities and cost performances of the conductors will be improved in accordance with various requirements in spreading area of applications.

As for compound superconductors, they are still in the stage of research and development, although the developments have been proceeding and lately accelerated owing to great demands for high field and high current density. The targets of short term are to develop high J_c conductors for high field magnet up to 20 tesla, and large capacity conductors for fusion reactor and high energy physics applications. The conductor, probably Nb₃Ge tape, for power transmission line operating at liquid hydrogen temperature is a target of long term.

The last conductors in Fig. 35 are a dream at present, but have some possibility left yet. Progress in material researches and new technologies in near future may bring forth developments of new superconductors. Consequently, it is emphasized that basic material research as well as advanced fabrication technology is extremely important for the expansive commercialization of superconductors and their applications. It goes without saying that close collaborations between the related people of materials and applications are desired for the developments above-mentioned.

Table VII. Processing methods for compound superconductors.

Processing techniques	Compounds
(1) Bronze process (solid state diffusion)	Nb ₃ Sn, V ₃ Ga, V ₃ Si, Nb ₃ Al
(2) Surface diffusion (liquid solute diffusion)	Nb ₃ Sn, Nb ₃ Al, Nb ₃ Ga, V ₃ Ga
(3) CVD (gas state reaction)	Nb ₃ Sn, Nb ₃ Ga, V ₃ Si, Nb ₃ Ge
(4) PD (electron beam and sputtering)	Nb ₃ Sn, Nb ₃ (Al, Ge), Nb ₃ Ge
(5) Reactive sputtering deposition	NbN, (Nb, Ti)N
(6) Powder metallurgy	Nb ₃ Sn, Nb ₃ Al, V ₃ Ga
(7) In-situ process	Nb ₃ Sn, V ₃ Ga

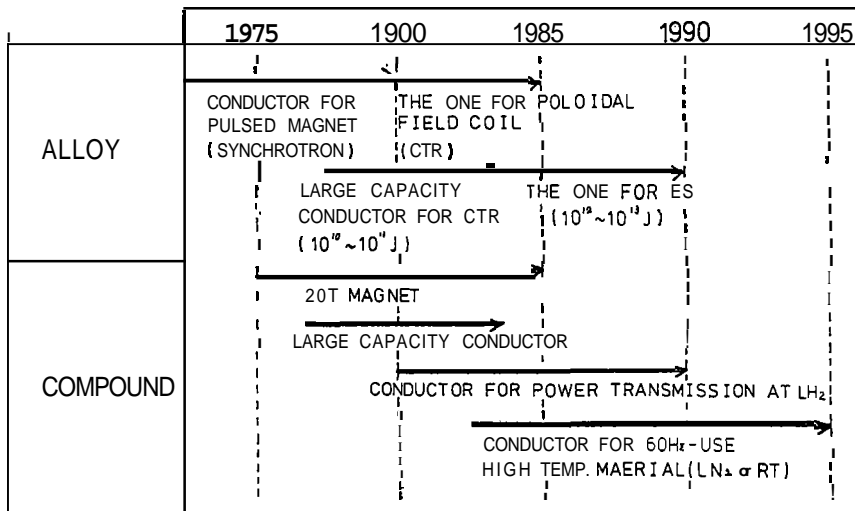


Figure 35. Prospects for superconductors in future.

Acknowledgements

The author's appreciation is extended to Y. Tanaka and S. Meguro, his colleagues, for much help in the preparation of this paper.

References

1. H. K. Onnes, Commun. Phys. Lab. Univ. Leiden Nos. 119b, 120b, 122b (1911), quoted in D. Shoenberg, Superconductivity, p. 1, Cambridge, New York, 1952.
2. J. K. Hulm and B. T. Matthias, "High-Field, High-Current Superconductors", Science, 208, (1980) pp. 881-887.
3. B. W. Roberts, "Superconducting Properties of Elements, Alloys, and Compounds", J. Phys. Chem. Ref Data, 5, (1976) p. 581.
4. G. F. Hardy and J. K. Hulm, "Superconducting Silicides and Germanides", Phys. Rev. 89, (4) (1953) pp. 884-886.
5. B. T. Matthias, T. H. Geballe, S. Geller, and E. Corenzwit, "Superconductivity of Nb_3Sn ", Phys. Rev., 95, (6) (1954) p. 1435.
6. J. E. Kunzler, "Superconductivity in High Magnetic Fields at High Current Densities", Rev. Mod. Phys., 33 (4) (1961) pp. 501-509.
7. T. H. Geballe and J. K. Hulm, "Superconducting Materials up to Now and into Future", IEEE Trans. on Magn., Mag-11 (2) (1975) pp. 119-124.
8. J. Bardeen, L. N. Cooper, and J. R. Schrieffer, "Theory of Superconductivity", Phys. Rev., 108 (5) (1957) pp. 1175-1204.
9. B. T. Matthias, "Superconductivity in the Periodic System", Prog. Low Temp. Phys., 2, (1957) pp. 138-150.
10. B. T. Matthias, "Superconductivity of Nb_2Ge ", T. H. Geballe, R. H. Willens, E. Corenzwit, and G. W. Hull, Jr., Phys. Rev., 139 (5A) (1965) pp. 1501-1503.
11. J. R. Gavaler, J. Appl. Phys. Lett., 23, (1973) p. 480.
12. S. Paidassi, J. Spitz, and J. Besson, "Chemical Vapor Deposition of Nb_3Ge on Continuous Stainless Steel Tapes", Appl. Phys. Lett., 33, (1978) pp. 105-107.
13. R. E. Somekh and J. E. Evetts, "The Sputtering of High T $A15 Nb_3Sn$ and V_3Ge ", Solid State Comm., 24 (10) (1977) pp. 733-737.
14. D. Dew-Hughes, "Superconducting Composites", Cryogenics 15 (8) (1975) pp. 435-454.
15. W. L. McMillan, "Transition Temperature of Strong-Coupled Superconductor", Phys. Rev., 167 (2A) (1975) pp. 331-344.
16. W. Meissner and R. Ochsenfeld, "Ein Neuer Effect bei Eintritt der Supraleitfähigkeit", Naturwissenschaften, 21, (1933) pp. 787-788.
17. B. B. Goodman, "The Magnetic Behavior of Superconductors of Negative Surface Energy", MB J. Rev. & Devel., 6 (1962) pp. 63-64.

18. Y. B. Kim, C. F. Hempstead, and A. R. Strnad, "Flux Flow Resistance in Type II Superconductor", *Phys. Rev.* 139 (4A) (1965) pp. 1163-1172.
19. S. Foner, E. J. McNiff, Jr., and E. J. Alexander, "High Field Properties of Ternary Metal-Molybdenum-Sulfides", *IEEE Trans. on Magn.*, **VAG-11** (2) (1975) pp. 155-158.
20. A. M. Clogston, "Upper Limit for the Critical Field in Hard Superconductors", *Phys. Rev. Lett.*, 9 (6) (1962) pp. 266-267.
21. N. R. Yerthamer, E. Helfand, and P. C. Hohenberg, "Temperature and Purity Dependence of Superconducting Critical Field, H_{c2} ", *Phys. Rev.*, 147 (1A) (1966) pp. 295-302.
22. M. Suenaga and K. M. Ralls, "Some Superconducting Properties of Ti-Nb-Ta Ternary Alloys", *J. Appl. Phys.*, 40 (11) (1969) pp. 4457-4463.
23. H. Sekine, T. Takeuchi, and K. Tachikawa, "Studies on the Composite Processed Nb-Hf/Cu-Sn-Ga High Field Superconductors", *IEEE Trans. on Magn.*, **MAG-17** (1981) pp. 383-386.
24. C. P. Bean, "Magnetization of Hard Superconductors", *Phys. Rev. Lett.* 8 (6) (1962) pp. 250-253.
25. J. E. Evetts, A. M. Campbell, and D. Dew-Hughes, "Forces on Flux Vortices in an Arbitrary Configuration", *J. Phys. C1* (3) (1968) pp. 715-731.
26. A. M. Campbell and J. E. Evetts, "Flux Vortices and Transport Currents in Type II Superconductors", *Adv. Phys.*, 21 (1972) pp. 199-428.
27. S. D. Dahlgren, "High-Rate Sputtering of Nb-Al-Ge and Nb-Al Superconductors", *IEEE Trans. on Magn.*, **MAG-11** (2) (1975) pp. 217-220.
28. E. J. Kramer, "Scaling Laws for Flux Pinning", *J. Appl. Phys.*, 44 (3) (1973) pp. 1300-1370.
29. A. W. West and D. C. Larbalestier, "Transmission Electron Microscopy of Commercial Filamentary Nb-Ti Superconducting Composites", *Adv. in Cryo. Eng.*, 26 (1980) pp. 471-478.
30. P. R. Critchlow, E. Gregory, and B. Zeitlin, "Multifilamentary Superconducting Composites", *Cryogenics*, 11 (1971) pp. 3-10.
31. J. Willbrand and W. Schlump, *Z. Metallkunde*, 66 (1975) p. 714.
32. T. Suzuki and Y. Furuto, "Effect of Heat Treatment on Superconducting Properties of Nb-Ti Alloys", *Proc. IIR Comm. I Meeting, Tokyo* (1970) pp. 173-179.
33. H. R. Segal, T. A. de Winter, Z. J. J. Stekly, and T. Hemachalam, "The Use of Nb-Ti-Ta as a High Field Superconducting Alloy", *IEEE Trans. on Magn.*, **MAG-17** (1981) pp. 53-56.
34. R. M. Scanlan, W. A. Fietz, and E. F. Koch, "Flux Pinning Centers in Superconducting Nb₃Sn", *J. Appl. Phys.*, 46 (5) (1975) pp. 2244-2249.

35. R. E. Enstrom and J. R. Appert, "Preparation, Microstructure, and High Field Superconducting Properties of Nb₃Sn Doped with Cr-II - V and III Elements", *J. Appl. Phys.*, **43** (4) (1972) pp. 1915-1923; **45** (1) (1974) pp. 421-428.
36. T. Luhman and M. Suenaga, "Improvements in Critical Current Densities of Nb₃Sn by Solid Solution Additions of Sn in Nb", *Adv. Cryo. Eng.*, **22** (1977) pp. 356-361.
37. M. N. Wilson, "Stabilization of Superconductors for Use in Magnets", *IEEE Trans. on Magn.*, **MAG-13** (1977).
38. Z. J. J. Stekly and E. Boag, "Effect of Cu Plating on Velocity of Propagation of Normal Region in Nb-25% Zr Wire", *J. Appl. Phys.* **34** (4) (1963) pp. 1376-1377.
39. S. Meguro, Y. Furuto, H. Yoshida, T. Suzuki, T. Itoh, and I. Inoue, "Improvements in Thermal Stability of the Conductor for Large Coil", *Proc. 8th Symp. Eng. Probl. Fusion Res.*, (1979) pp. 1416-1420.
40. R. Hancox, *Proc Int. Congr. Low-Temp. Phys.* 10th 2, (1966) p. 43.
41. S. L. Wipf and M. S. Lubell, "Flux Jump in Nb-25%Zr under Nearly Adiabatic Conditions", *Phys. Lett.*, **16** (2) (1965) pp. 103-105.
42. M. N. Wilson, C. R. Walters, J. D. Lewin, and P. F. Smith, "Experimental and Theoretical Studies of Filamentary Superconducting Composites", *J. Phys.*, **D3** (1970) pp. 1517-1546.
43. G. H. Morgan, "Theoretical Behavior of Twisted Multicore Superconducting Wire in Time-Varying Uniform Magnetic Field", *J. Appl. Phys.* **41** (9)(1970) pp. 3673-3679.
44. Y. Furuto, T. Suzuki, K. Tachikawa, and Y. Iwasa, "Current-Carrying Capacities of Superconducting Multifilamentary V₃Ga Cables", *Appl. Phys. Lett.*, **24** (1974) pp. 34-36.
45. Y. Tanaka, Y. Furuto, M. Ikeda, I. Inoue, T. Suzuki, and S. Meguro, "Multifilamentary Stranded Compound Superconductors", *Cryogenics*, **17** (1977) pp. 233-241.
46. J. Silcox, "Hysteresis in Hard Superconductors", *Rev. Mod. Phys.*, **36** (1) (1964) pp. 52-54.
47. F. Irie and K. Yamafuji, "Theory of Flux Motion in Non-Ideal Type II Superconductors", *J. Phys. Soc. Japan*, **23** (2) (1967) pp. 255-268.
48. Y. Furuto, T. Suguki, M. Ikeda, S. Meguro, and Y. Tanaka, "Fabrication of Superconductors for Synchrotron", *Proc. 1st Symp. on Accel. Sci. & Tech.* (1970) pp. 173-174.
49. H. Brechna, Tokyo "Superconducting Magnets" pp. 139-217 in "Superconducting Machines and Devices", S. Foner and B. B. Swartz, eds. Plenum Press, New York, 1974.
50. W. J. Carr, Jr., "Parallel Field Losses in Twisted Multifilament Superconductors", *Proc. 6th Symp. on Fusion Eng.*, (1975) pp. 152-155.

51. B. Turck, "Experimental and Theoretical Approach of Current Distribution and Losses in Superconducting Composites for Fusion Magnets", IEEE Trans. Magn. MAG-13 (1) (1977) pp. 548-551.
52. R. W. Meyerhoff and W. T. Beall, Jr., "High-Current AC Losses in Large Superconducting Nb Tubes", J. Appl. Phys. 42 (1) (1971) pp. 147-153.
53. C. N. Carter and J. Sutton, "Solenoids of Composite Conductor Simulate AC Losses in Flexible Superconducting Cable", Cryogenics, 15 (10) (1975) pp. 599-607.
54. Y. Furuto, T. Miura, M. Ikeda, and I. Inoue, "Electrical Test on Superconducting Model Cable", Proc. ICEC5, (1974) pp. 180-183.
55. J. F. Bussiere, "Development of Low-Loss Nb₃Sn for AC Power Transmission", IEEE Trans. Magn., MAG-13 (1) (1977) pp. 131-137.
56. S. Meguro, Y. Furuto, T. Suzuki, M. Ikeda, Y. Tanaka and I. Inoue, "Three-Component Composite Superconductor", Proc. ICEC5 (1974) pp. 504-507.
57. R. Yamada, H. Ishimoto, and M. E. Price, "Superconducting Wire Test", IEEE Trans. Magn. MAG-13 (1) (1977) pp. 552-555.
58. S. S. Shen, "Magnetic properties of Multifilamentary Nb₃Sn Composites", Proc. Topical Conf. on Al5 Supercon. (ICMC), (1980) pp. 309-320.
59. C. C. Koch and D. S. Easton, "A Review of Mechanical Behavior and Stress Effects in Hard Superconductors", Cryogenics, 17 (1977) pp. 391-413.
60. Y. Furuto and S. Meguro, "Cryostable Superconductors in Energy Storage Systems", Intern. Symp. Supercon. Energy Storage, Osaka (1979) pp. 205-209.
61. T. Luhman and M. Suenaga, "Effects of Stresses, Induced by Thermal Contraction of a Bronze Matrix, on the Superconducting Properties of Nb₃Sn Tapes", Appl. Phys. Lett., 29 (1) (1976) pp. 61-63.
62. G. Rupp, "The Importance of Being Prestressed", Proc. Topical Conf. on Al5 Supercon. (ICMC), (1980) pp. 155-170.
63. J. W. Ekin, "Strain Scaling Law and Prediction of Uniaxial and Bending Strain Effects in Multifilamentary Superconductors", *ibid.* (1980) pp. 187-204.
64. R. M. Scanlan, R. W. Hoard, D. N. Cornish, and J. P. Zbasnik. "Mechanical Properties of High-Current Multifilamentary Nb₃Sn Conductors", *ibid.* (1980) pp. 221-231.
65. Y. Furuto, Y. Tanaka, S. Meguro, T. Suzuki, and I. Inoue, "Development of Multifilamentary Compound Superconductors", *ibid.* (1980) pp. 115-130.
66. Y. Furuto and M. Ikeda, "Contact Resistance of Stabilized Superconducting Wires", Proc. ICEC2, (1968) pp. 179-183.